NIST-GCR-88-553

Radiation from Turbulent Nonluminous and Luminous Diffusion Flames

Y. R. Sivathanu, M. E. Kounalakis, J. P. Gore and G. M. Faeth

University of Michigan
Department of Aerospace
Engineering
Ann Arbor, MI

October 1987

Issued October 1988

Prepared for
U.S. DEPARTMENT OF COMMERCE
National Institute of Standards
and Technology
(Formerly National Bureau of Standards)
National Engineering Laboratory
Center for Fire Research
Gaithersburg, MD 20899

75 Years Stimulating America's Progress
1913-1988

NIST-GCR-88-553

Radiation from Turbulent Nonluminous and Luminous Diffusion Flames

Y. R. Sivathanu, M. E. Kounalakis, J. P. Gore and G. M. Faeth

University of Michigan
Department of Aerospace
Engineering
Ann Arbor, MI

October 1987

Issued October 1988

NIST Grant No. 60NANB5D0576

National Bureau of Standards became the
National Institute of Standards and Technology
on August 23, 1988, when the Omnibus Trade and
Competitiveness Act was signed. NIST retains
all NBS functions. Its new programs will encourage
improved use of technology by U.S. industry.

Prepared for
U.S. DEPARTMENT OF COMMERCE
National Institute of Standards
and Technology
(Formerly National Bureau of Standards)
National Engineering Laboratory
Center for Fire Research
Gaithersburg, MD 20899

U.S. DEPARTMENT OF COMMERCE
C. William Verity, Secretary

NATIONAL INSTITUTE OF STANDARDS
AND TECHNOLOGY
Ernest Ambler, Director

Notice

This report was prepared for the Center for Fire Research of the National Engineering Laboratory, National Bureau of Standards, under Grant Number 60NANB5D0576. The statements and conclusions contained in this report are those of the authors and do not necessarily reflect the views of the National Bureau of Standards or the Center for Fire Research.

RADIATION FROM TURBULENT NONLUMINOUS AND LUMINOUS DIFFUSION FLAMES

Y. R. Sivathanu, M. E. Kounalakis, J. P. Gore
and G. M. Faeth

The University of Michigan
Department of Aerospace Engineering
Ann Arbor, MI 48109-2140

Annual Report: Grant No. 60NANB5D0576

October 1987

Sponsored by

U. D. Department of Commerce
National Bureau of Standards
Center for Fire Research
Washington, DC 20234

RADIATION FROM NONLUMINOUS AND LUMINOUS TURBULENT DIFFUSION FLAMES

October 1987

Sponsored by:
U.S. Department of Commerce
National Bureau of Standards
Center for Fire Research
Washington, DC 20234

ABSTRACT

A theoretical and experimental study of the structure and radiation properties of turbulent buoyant diffusion flames is described. The results have application to modeling fires within structures, materials test methods, fire detection, and effects of materials on fire properties.

The investigation consists of two phases, as follows: study of effects of turbulence/radiation interactions, considering the properties of nonluminous hydrogen/air diffusion flames; and study of extension of the laminar flamelet concept to soot properties needed to predict radiation from luminous acetylene/air and ethylene/air turbulent diffusion flames. Theory and experiment are considered in both phases of the investigation.

Measurements in turbulent hydrogen/air diffusion flames yielded radiation fluctuation intensities of 20-110 percent, providing direct evidence of the importance of turbulence/radiation interactions. A stochastic analysis, based on the laminar flamelet concept, was developed which provided encouraging predictions of mean and fluctuating spectral radiation intensities (average discrepancies between predictions and measurements were roughly 30 percent), as well as temporal power spectral densities of radiation fluctuations. The temporal spectra exhibit energy-containing and inertial regions, very similar to other turbulence properties, although the rate of decay of the spectra with increasing frequency in the inertial region is somewhat greater than observed for scalar fluctuations.

Measurements and predictions in the turbulent luminous flames concentrated on scalar properties (particularly soot volume fractions) in the overfire region. Predictions of scalar properties based on the laminar flamelet concept were very encouraging. Direct evaluation of soot volume fraction state relationships for the overfire region was hampered by effects of turbulent fluctuations and experimental uncertainties; nevertheless, within these limitations, soot volume fraction state relationships were nearly universal, and soot generation efficiencies nearly constant, for sufficiently long residence times. However, effects of finite-rate chemistry were noted for short residence time ethylene/air flames, causing spatial variations of soot generation efficiencies in the overfire region. For long residence times, present measurements of soot generation efficiencies were in reasonably good agreement with earlier findings for acetylene/air and ethylene/air diffusion flames.

ACKNOWLEDGEMENT

This research was supported by the United States Department of Commerce, National Bureau of Standards, Grant Number 60NANB5D0576, with D. D. Evans and J. B. McCaffrey of the Center for Fire Research serving as Scientific Officers.

TABLE OF CONTENTS

Page

Abstract iv

Acknowledgements v

List of Tables viii

List of Figures ix

Nomenclature xii

1. Introduction 1

2. Nonluminous Flames 3

  2.1 Introduction 3

  2.2 Experimental Methods 4
    2.2.1 Apparatus 4
    2.2.2 Instrumentation 4
    2.2.3 Test Conditions 6

  2.3 Theoretical Methods 7
    2.3.1 Structure Analysis 7
    2.3.2 Radiation Analysis 10

  2.4 Results and Discussion 12
    2.4.1 Flame Structure 12
    2.4.2 Mean Radiation Properties 16
    2.4.3 Radiation Fluctuations 19

  2.5 Summary 31
    2.5.1 Conclusions 31
    2.5.2 Plans 32

3. Luminous Flames 34

  3.1 Introduction 34

TABLE OF CONTENTS (continued)

Page

3.2 Experimental Methods 37
3.2.1 Apparatus 37
3.2.2 Instrumentation 37
3.2.3 Test Conditions 38

3.3 Theoretical Methods 40

3.4 Results and Discussion 40
3.4.1 Acetylene/Air Flames 40
3.4.2 Ethylene/Air Flames 54
3.4.3 Soot Generation Efficiencies 67

3.5 Summary 69
3.5.1 Conclusions 69
3.5.2 Plans 70

References 72

LIST OF TABLES

Table	Title	Page
1	Test Conditions for Hydrogen/Air Diffusion Flames	7
2	Mean Spectral Radiation Intensities (W/cm^2 sr μm) for Hydrogen/Air Diffusion Flames	24
3	Intensity of Spectral Radiation Intensity Fluctuations (Percent) for Hydrogen/Air Diffusion Flames	25
4	Test Conditions for Laminar Diffusion Flames	39
5	Soot Generation Efficiencies	68

LIST OF FIGURES

Figure	Caption	Page
1	Sketch of burner apparatus.	5
2	State relationships for hydrogen/air diffusion flames.	9
3	Sketch of temporal simulation of eddy properties.	13
4	Properties along axis of hydrogen/air diffusion flame (Re = 5,720).	14
5	Properties along axis of hydrogen/air diffusion flame (Re = 3,000).	15
6	Mean spectral radiation intensities for hydrogen/air diffusion flame (Re = 5,720).	17
7	Mean spectral radiation intensities for hydrogen/air diffusion flame (Re = 3,000).	18
8	Effect of characteristic eddy size on spectral radiation intensity fluctuations.	20
9	Effect of characteristic eddy size on the power spectrum of spectral radiation intensity fluctuations (Re = 3,000, x/d = 50).	22
10	Probability density of normalized spectral radiation intensities for hydrogen/air diffusion flame (Re = 5,720).	26
11	Probability density of normalized spectral radiation intensities for hydrogen/air diffusion flame (Re = 3,000).	27
12	Power spectra of spectral radiation intensity fluctuations for hydrogen/air diffusion flame (Re = 5,720).	29
13	Power spectra of spectral radiation intensity fluctuations for hydrogen/air diffusion flame (Re = 3,000).	30
14	Properties along axis of acetylene/air diffusion flame (Re = 9,200).	41
15	Properties along axis of acetylene/air diffusion flame (Re = 5,300).	42
16	Mean mixture fraction distributions in acetylene/air diffusion flames.	44

LIST OF FIGURES (continued)

Figure Caption Page

17 Mean gas species concentrations in acetylene/air diffusion flames (x/d = 53). 45

18 Mean gas species concentrations in acetylene/air diffusion flames (x/d = 80). 46

19 Mean gas species concentrations in acetylene/air diffusion flames (x/d = 110). 47

20 Mean gas species concentrations in acetylene/air diffusion flames (x/d = 130). 48

21 Mean soot volume fraction distributions in acetylene/air diffusion flames. 50

22 Correlation between soot volume fractions and mixture fractions in the overfire region of acetylene/air diffusion flames (the stoichiometric mixture fraction is 0.0702). 51

23 Soot volume fraction state relationship for acetylene/air diffusion flames (the stoichiometric mixture fraction is 0.0702). 53

24 Properties along axis of ethylene/air diffusion flame (Re = 12,740). 55

25 Properties along axis of ethylene/air diffusion flame (Re = 6,370). 56

26 Mean mixture fraction distributions in ethylene/air diffusion flames. 57

27 Mean gas species concentrations in ethylene/air diffusion flames (x/d = 50). 58

28 Mean gas species concentrations in ethylene/air diffusion flames (x/d = 70). 59

29 Mean gas species concentrations in ethylene/air diffusion flames (x/d = 90). 60

30 Mean gas species concentrations in ethylene/air diffusion flames (x/d = 130). 61

LIST OF FIGURES (continued)

Figure	Caption	Page
31	Mean gas species concentrations in ethylene/air diffusion flames (x/d = 150).	62
32	Mean soot volume fraction distributions in ethylene/air diffusion flames.	63
33	Correlation between soot volume fractions and mixture fractions, in the overfire region of ethylene/air diffusion flames (the stoichiometric mixture fraction is 0.0634).	65
34	Soot volume fraction state relationships for ethylene/air diffusion flames (the stoichiometric mixture fraction is 0.0634).	66

NOMENCLATURE

Symbol	Description
a	acceleration of gravity
C_e	ratio of characteristic eddy length to dissipation length scales
C_μ	turbulence model constant
d	burner exit diameter
$E(f)$	power spectral density of spectral radiation intensity fluctuation
f	mixture fraction, frequency
f_v	soot volume fraction
g	square of mixture fraction fluctuations
i	$(-1)^{1/2}$
i_λ	spectral radiation intensity
I_λ	Fourier transform of spectral radiation intensity
k	turbulent kinetic energy
m_o	burner mass flow rate
L_e	characteristic eddy length scale
L_{eb}	baseline characteristic eddy length scale
p	pressure
$P(f)$	probability density function of f
$\dot{Q}$	heat release rate
$\dot{Q}_{rad}$	radiative energy loss from flame to surroundings
r	radial distance
R_λ	autocorrelation of spectral radiation intensity fluctuations
Re	burner Reynolds number
Ri	burner Richardson number
t	time

t_e	characteristic eddy lifetime
T	temperature, end of time interval
u	streamwise velocity
v	radial velocity
w	tangential velocity
x	height above burner
Y_i	mass fraction of species i
ε	rate of dissipation of turbulence kinetic energy
λ	wavelength
μ_{eff}	effective viscosity
μ_t	turbulent viscosity
υ	kinematic viscosity
ρ	density
ϕ	generic property, fuel equivalence ratio

Subscripts

c	centerline value
o	burner exit condition
∞	ambient condition

Superscripts

$(\bar{\ })$	time-averaged quantity
$(\tilde{\ })$	Favre-averaged quantity
$(\bar{\ })'$	root-mean-squared time-averaged fluctuating quantity
$(\tilde{\ })''$	root-mean-squared Favre-averaged fluctuating quantity

1. INTRODUCTION

Radiation from turbulent flames is an important heat transfer mechanism for fires. Radiant transport influences the rate of burning of objects already on fire, the rate of spread of the fire, and the rate of heating of surrounding structural elements. In spite of significant progress, substantial gaps exist in current understanding of the structure and radiation properties of turbulent flames. The objective of the present study is to investigate these properties for both nonluminous and luminous (nonsooting and sooting) buoyant turbulent diffusion flames. The results of the research have application to modeling fires within structures, materials test methods, fire detection, and effects of materials on fire properties.

Two aspects of radiation from buoyant turbulent diffusion flames are being considered. The first relates to turbulence/radiation interactions i.e., the effect of the intrinsic unsteadiness of turbulent flames on their radiation properties. Past work has shown that these interactions are important for nonluminous and luminous flames, frequently yielding radiative heat fluxes more than 100 percent higher than estimates based on time-averaged scalar properties in the flame (Cox, 1977; Gore and Faeth, 1987a,b; Gore et al., 1987a,b,c; Jeng et al, 1984; Kabashnikov and Kmit, 1979). A stochastic method for treating these interactions has been developed in this laboratory (Jeng et al., 1984). The approach seems promising for estimating effects of turbulence/radiation interactions, however, aspects of the method are ad hoc and past evaluations have been indirect, based on differences between mean-property and stochastic predictions and their comparison with measurements of mean radiation properties. Thus, in order to gain more insight concerning turbulence/radiation interactions, radiation fluctuations from flames were examined directly, and related to fluctuations of scalar properties, during the present study. The objective was to provide direct evidence of turbulence/radiation interactions and to advance stochastic methods to treat this phenomenon.

The second aspect of the investigation relates to the laminar flamelet concept for soot volume fractions, i.e., whether there are universal relationships between soot volume fractions (the main soot property needed for radiation predictions in luminous flames), and mixture fractions (the fraction of mass at a point which originated from the fuel), for various fuels burning in air. There is some evidence in the literature that such relationships may exist for the buoyant flames encountered in unwanted fires (Becker and Liang, 1982, 1983; Gore and Faeth, 1987a,b; Kent, 1987; Kent and Bastin, 1984). If this proves to be true, problems of estimating soot volume fractions in turbulent flames would be vastly simplified, circumventing the enormous difficulties of treating soot chemistry in turbulent flame environments. Thus, a second objective of the study was to undertake measurements and analysis to examine the viability of the laminar flamelet concept for soot volume fractions, emphasizing the overfire region of acetylene/air and ethylene/air diffusion flames.

Progress on each aspect of the study is described in the following. The discussion begins with nonluminous flames, which have been used to initiate work on turbulence/radiation interactions; and then turns to luminous flames, which are being considered in order to examine the laminar flamelet concept for soot volume fractions.

2. NONLUMINOUS FLAMES

2.1 Introduction

Similar to other properties of turbulent diffusion flames, radiation emitted from the flame varies in time, even when mean properties are stationary. This is a direct manifestation of turbulence/radiation interactions. The existence of temporal variations or fluctuations of flame radiation is widely recognized. For example, radiation fluctuations are frequently exploited during the design of fire and combustion plume detection systems, where the temporal radiation signature provides a means of distinguishing flames from background radiation. Naturally, the rational design of such devices requires an understanding of flame radiation fluctuations. Furthermore, the temporal properties of flame radiation fluctuations provide a unique perspective for gaining a better understanding of turbulence/radiation interactions in flames, similar to the perspective provided by the temporal properties (power spectra) of velocity and concentration fluctuations in a turbulent flow. Motivated by these considerations, the temporal properties of radiation fluctuations from turbulent diffusion flames were examined, both theoretically and experimentally, during this phase of the investigation. Only nonluminous flames were considered, in order to minimize uncertainties due to soot processes in turbulent flame environments.

Turbulence/radiation interactions in diffusion flames have recently attracted attention. Cox (1977) and Kabashnikov and Kmit (1979) used simplified radiation models of flames to show that turbulent fluctuations could cause significant increases of mean radiation levels from estimates based on mean scalar properties. Subsequently, the radiation properties of nonluminous and luminous turbulent diffusion flames were studied in this laboratory, considering hydrogen (Gore et al., 1987c), carbon monoxide (Gore et al., 1987b), methane (Jeng et al., 1984), natural gas (Gore et al., 1987a), ethylene (Gore and Faeth, 1987a) and acetylene (Gore and Faeth, 1987b) flames, all burning in still air. A stochastic method for treating turbulence/radiation interactions was developed during these studies, which yielded encouraging agreement with measurements of mean spectral radiation intensities and radiative heat fluxes. These findings confirmed that turbulence/radiation interactions caused substantial (more than 100 percent) increases of flame radiation above estimates based on mean scalar properties, for most flame systems. A theoretical objective of the present investigation was to see whether these ideas could be extended to treat the temporal properties of flame radiation fluctuations.

Porscht (1978) has reported virtually the only measurements of the temporal properties of flame radiation fluctuations in the literature. This involved measurements of the power spectral densities of the output of several flame radiation detectors, which were viewing buoyant turbulent diffusion flames. These results clearly show relatively large radiation fluctuations in comparison to mean radiation levels, experimentally demonstrating the importance of turbulence/radiation interactions. However, the radiation wavelength and temporal response of the detectors, and the scalar properties of the flames, were not well defined; therefore, the results provide only limited quantitative information concerning the relationship between scalar property and radiation fluctuations of flames. The present study extends the experimental work of Porscht (1978) by considering specific wavelength and calibrated detectors capable of resolving the temporal frequency range of the radiation, as well as turbulent flames whose structure was known from earlier studies.

The report of this phase of the study begins with a description of experimental and theoretical methods. Measurements and predictions are then discussed. This part of the report ends with conclusions that can be drawn from results obtained thus far, and a description of plans for ongoing research concerning turbulence/radiation interactions.

2.2 Experimental Methods

2.2.1 Test Apparatus

Except for the radiation measurements, experimental methods were similar to past work (Gore and Faeth, 1987a,b; Gore et al., 1987b,c; Jeng and Faeth, 1984a,b,c; Jeng et al., 1982, 1984) and will only be briefly described. The apparatus and instrumentation will be described first, followed by a summary of test conditions.

A sketch of the burner arrangement appears in Fig. 1. The tests were conducted in a room 4 m × 4 m × 10 m high, while the walls of this room were only 2.5 m high. Exhaust products were removed from the ceiling area using a blower. The burner was directed vertically upward within a screened enclosure (1.1 m × 1.2 m × 2.7 m high, one layer of screen, 630 wires/m, 0.25 mm wire diameter). The burner was maintained within ± 0.5 K of room temperature by water cooling. The fuel entered a baffled and screened plenum and then passed through a 25:1 contraction, designed to yield uniform exit velocities.

Fuel gas flow rates were measured using a laminar flow element, which was calibrated with a wet-test meter. The burner could be traversed in a horizontal direction along with the cage, and in a vertical direction within the cage, to facilitate measurements using rigidly-mounted optical instrumentation.

2.2.2 Instrumentation

The structure of the hydrogen/air flames was measured by Gore et al. (1987c). These measurements included the following: time-averaged mean and fluctuating streamwise velocities, using laser Doppler anemometry (LDA); mean gas species concentrations, by sampling and analysis with a gas chromatograph; mean temperatures, using fine-wire thermocouples; mean radiative heat fluxes, using a wide-angle radiometer; and mean spectral radiation intensities, using infrared spectroscopy. Aside from limited testing to check that

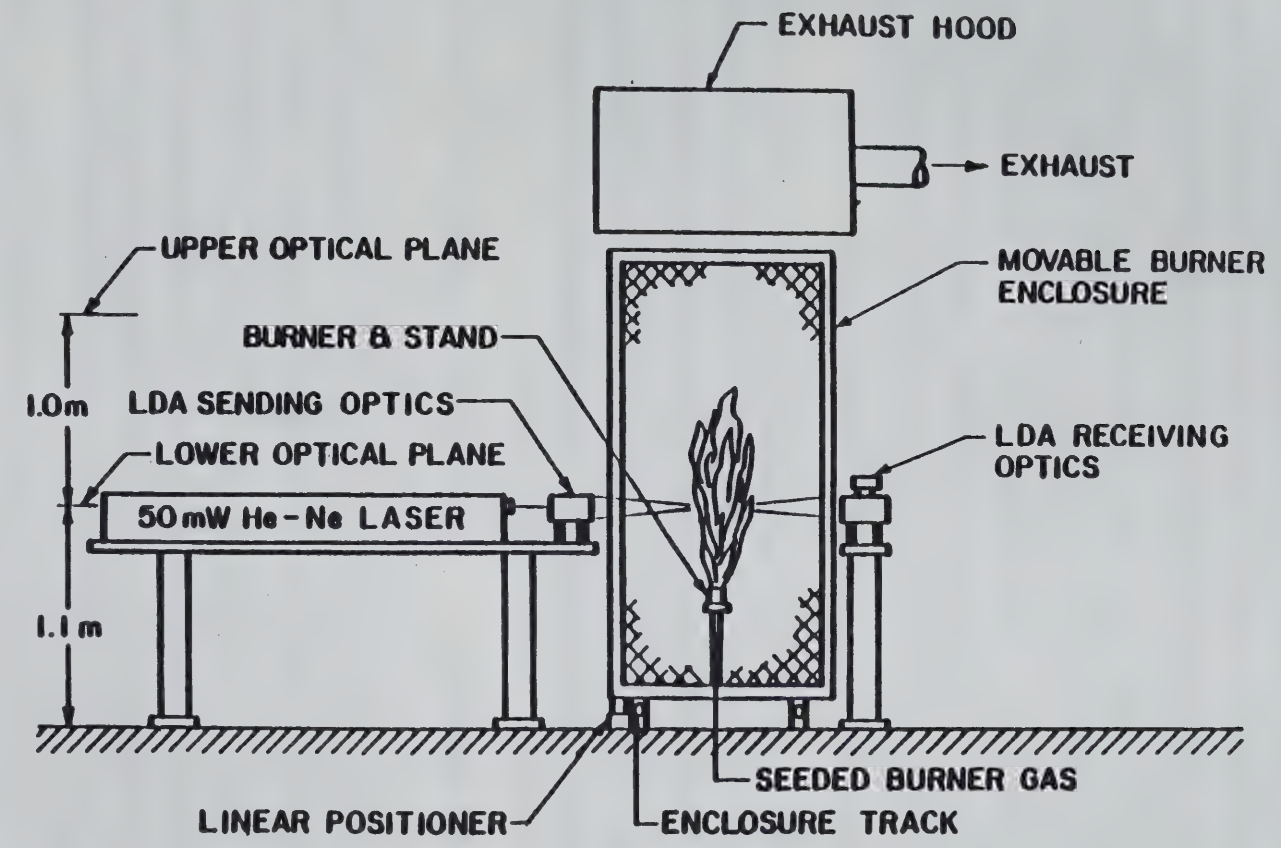

Figure 1. Sketch of burner apparatus.

earlier flame conditions had been reproduced, present measurements were limited to infrared spectroscopy and only these measurements will be discussed in the following. Complete details concerning the other measurements are provided by Gore (1986).

Spectral radiation intensities were measured for horizontal paths through the flame axis, at various heights above the burner exit. Two fields of view were used: a 10 mm diameter path with a 1.2 deg field angle, and a 5 mm diameter path with a 0.6 deg field angle. The larger diameter path is comparable to typical dissipation length scales within the flames, and is generally less than 25 percent of typical integral length scales. Two monochromators were used: a 750 mm Spex Model 1702, and an Oriel Model 7240. A PbS detector (New England Photomultiplier), operating at room temperature, and an 800 Hz chopper, were used with both instruments. The detector output was smoothed with a second-order filter having a break frequency of 250 Hz. A combination of gratings and order-sorting filters provided observations in the 1200-4000 nm wavelength range. However, measurements of the temporal properties of the spectral radiation intensities were made near a strong system of lines at 2520 nm, within the 2700 nm band of water vapor. At this condition, the Spex Model 1702 had a slit width of 4.8 nm while the Oriel Model 7240 had a slit width of 40 nm.

The system functions of the monochromators were calibrated using a black-body source (Infrared Industries, Model 463). Wavelength readings were calibrated using lines generated by a mercury lamp, the 632.8 nm lines of an HeNe laser, and their harmonics. Experimental uncertainties (95 percent confidence) of these measurements were less than 20 percent, and were repeatable within this range during the course of the experiments. In addition, earlier measurements of time-averaged spectral radiation intensities for these flames (Gore et al., 1987c) were successfully repeated, within 10 percent.

2.2.3 Test Conditions

Operating conditions for the hydrogen/air diffusion flames, which were identical to those studied by Gore et al. (1987c), are summarized in Table 1. Relatively high burner Reynolds numbers were used and flow disturbances within the burner were significant; therefore, the flow at the burner exit was turbulent, as evidenced by the relatively high levels of turbulence kinetic energy at the exit. Initial Richardson numbers were relatively low, however, effects of buoyancy were still significant over much of the region where measurements were made, since the ambient environment was still. Overall radiant heat losses were modest for both flames, ca. 10 percent, and were relatively independent of the burner Reynolds number, typical of buoyant turbulent diffusion flames (de Ris, 1978).

Information concerning initial conditions for the flames was obtained by measurements of $\bar{u}$, $\bar{u}'$ and $\bar{v}'$ at x/d = 2, which was the axial position nearest the burner exit accessible to the present LDA optics. The turbulence kinetic energy, k, was computed from these results, assuming $\overline{w'} = \overline{v'}$. These measurements are summarized by Gore (1986).

Table 1. **Test Conditions for Hydrogen/Air Diffusion Flames**[a]

Reynolds Number[b]	5722	3000
Richardson Number[c]	0.4×10^{-5}	1.5×10^{-5}
Measured u_o(m/s)	108.4	66.3
$k_o^{1/2} / u_o$	0.23	0.184
$\dot{Q}$(kW)	23.8	12.5
$\dot{Q}_{rad} / Q$(%)	8.7	10.2
Hydrogen Flow Rate (mg/s)[d]	200	105

[a] Flow directed vertically upward from a 5-mm diameter passage, in still air at NTP.

[b] $Re = u_o d / \upsilon$ based on fuel-gas properties at exit.

[c] $Ri = ad / u_o^2$.

[d] Commercial Grade, Linde Division of Union Carbide.

2.3 Theoretical Methods

2.3.1 Structural Analysis

The flame structure analysis is only briefly described in the following, since the approach was not changed from past methods (Gore and Faeth, 1987a,b; Gore et al., 1987a,b,c,d; Jeng and Faeth, 1984a,b; Jeng et al., 1982, 1984).

The model considers a steady, axisymmetric, turbulent jet in an infinite stagnant environment, under the boundary-layer approximations. The formulation is based on Favre-(mass weighted) averaged quantities, defined as follows:

$$\tilde{\phi} = \overline{\rho\phi} / \bar{\rho} \tag{2.1}$$

where an overbar represents a conventional time average (Bilger, 1976). Flow velocities are low in most natural fires; therefore, viscous dissipation, and kinetic energy are ignored in the mean flow equations – with little error. Typical of most models of turbulence, the exchange coefficients of all species and heat are assumed to be the same. At this stage, no attempt was made to consider coupling between radiation and flow properties, which would require combined solution of the governing equations of conservation of energy and radiative transfer. Instead, radiation was treated as a perturbation, only correcting the energy release of reaction to account for heat loss from the flame by radiation. This is quite reasonable for the present hydrogen/air diffusion flames, since they only lose roughly 10 percent of their chemical energy release by radiation, see Table 1. Turbulence properties were estimated using modeled governing equations for k, ε and g, based on past practice (Jeng and Faeth, 1984a,b). To reduce empiricism, however, turbulence/buoyancy interactions were ignored in the k and ε equations. Past work has shown that this approach still yields reasonably good predictions of mean properties, although, turbulence levels tend to be underestimated by 20-30 percent (Jeng et al., 1982).

Mixture fraction is a conserved scalar of present flows. Under the above assumptions, all instantaneous scalar properties are only a function of mixture fraction – called the state relationships. State relationships were developed using data from laminar flames, treating properties in a turbulent flame as the result of a succession of laminar flamelets passing a given location, e.g., the laminar flamelet method (Bilger, 1976, 1977). This concept is based on the observation by Bilger (1977), that the scalar properties within laminar flames are relatively universal functions of mixture fraction (for a relatively wide range of flame stretch rates, except near points of flame attachment), even when scalar properties depart from local thermodynamic equilibrium.

The state relationships for hydrogen/air diffusion flames, with the reactants initially at normal temperature and pressure, were correlated earlier by Gore et al. (1987c). The results are plotted in Fig. 2 as a function of the local fuel equivalence ratio (which is a single-valued function of mixture fraction). Predicted and measured data on the plot include the following: sampling measurements in laminar flames by Gore et al. (1987c); Raman spectroscopy measurements in laminar flames by Aeschliman et al. (1979); Raman spectroscopy measurements in turbulent flames by Drake et al. (1980), 1984); concentration and temperature predictions in laminar flames by Miller and Kee , (1977); and predictions based on the assumption of local adiabatic thermodynamic equilibrium, using the Gordon and McBride (1971) algorithm. The concentration measurements of Gore et al. (1987c) and Drake et al. (1980, 1984) are close to equilibrium predictions, which is not surprising since hydrogen/oxygen kinetics are known to be fast (Bilger, 1976). The temperature measurements of Drake et al. (1980, 1984), however, are somewhat below adiabatic equilibrium predictions, which they attribute to effects of finite-rate chemistry, causing superequilibrium concentrations of OH, in their high-speed coflowing jets. The earlier results of Aeschliman et al. (1979) and

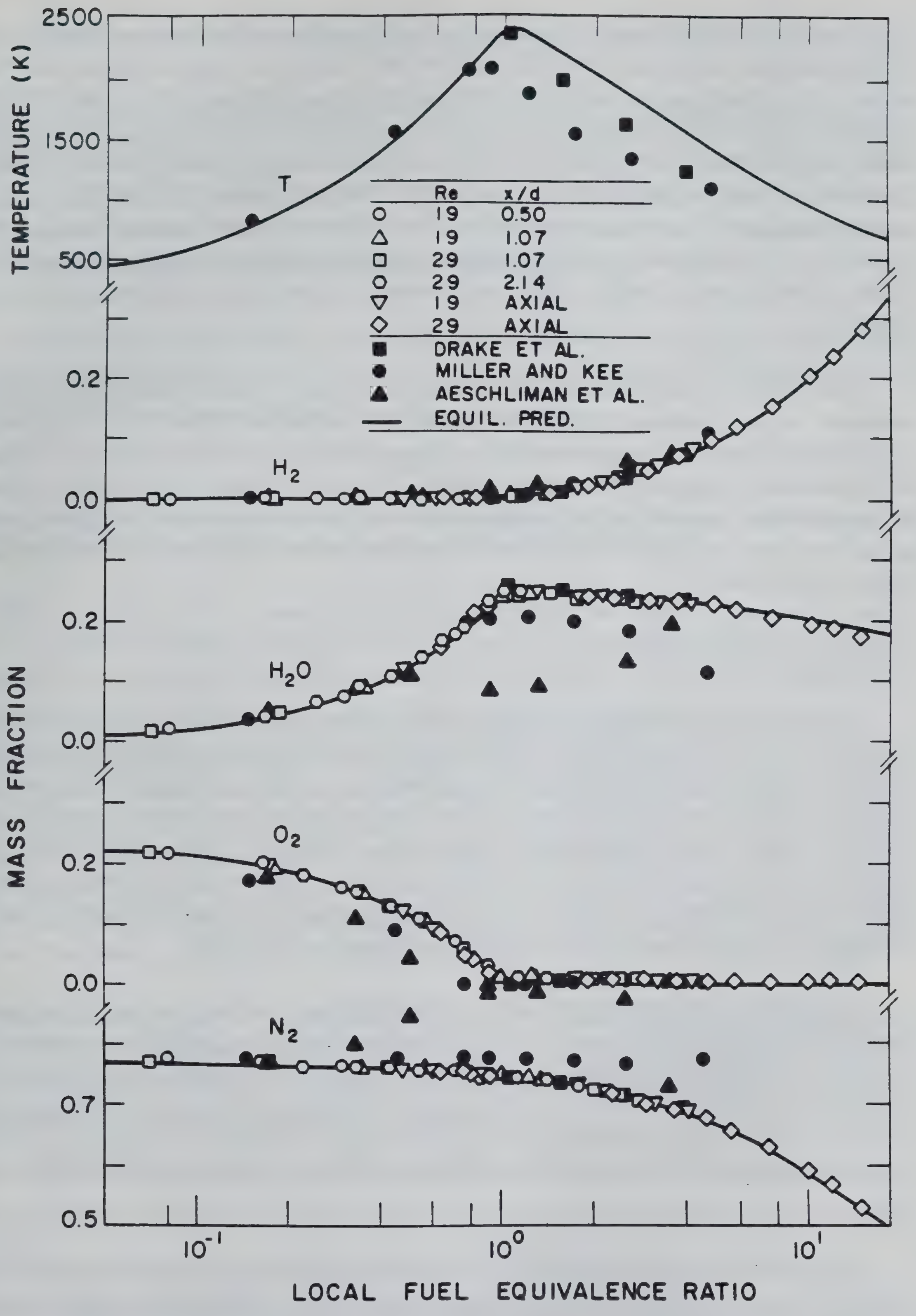

Figure 2. State relationships for hydrogen/air diffusion flames.

Miller and Kee (1977) diverge appreciably from equilibrium predictions, however, these findings are not supported by more recent work. Since the present flames have larger residence times and greater radiative heat losses than those of Drake et al. (1980, 1984), the procedure adopted for constructing state relationships was to ignore effects of OH superequilibrium but to allow for radiative heat losses during thermodynamic equilibrium calculations. The resulting state relationships for the composition of major gas species are virtually identical to the thermodynamic equilibrium predictions illustrated in Fig. 2, while temperatures are somewhat lower. Fortunately, uncertainties in gas temperatures are much less critical for predictions of radiation from nonluminous gas bands than is the case for blackbody radiation.

The governing equations appear in Jeng and Faeth (1984a) including all empirical constants – which were not changed for present computations. Time- and Favre-averaged scalar properties were computed assuming a clipped Gaussian probability density function for the Favre-averaged probability density function of mixture fraction. For the present flames, initial conditions were measured as discussed in the previous section. Computations were carried out using the GENMIX algorithm of Spalding (1977), with numerical closure achieved similar to past work.

2.3.2 Radiation Analysis

Spectral radiation intensities were found by solving the equation of radiative transfer for the optical paths and spectral ranges viewed by the monochromators. A narrow-band analysis was used, ignoring scattering, following Ludwig et al. (1973). This involves the Goody statistical narrow-band model along with the Curtiss-Godson approximation to account for absorption effects along inhomogeneous gas paths. The 1140, 1380, 1870, 2700 and 6300 nm gas bands of water vapor were considered, although computations of temporal radiation properties were limited to the 2700 nm band. The computations of spectral radiation intensities were carried out using the RADCAL algorithm of Grosshandler (1980).

In order to check present calculations with earlier work, calculations were also completed using time-averaged scalar properties along the radiation path – neglecting turbulence/radiation interactions. The bulk of present calculations, however, considered turbulence/radiation interactions using stochastic methods. This involved extending the approach developed earlier in this laboratory (Gore and Faeth, 1987a,b; Gore et al. 1987a,b,c,d; Jeng et al., 1984) to provide estimates of both the spatial and temporal variation of scalar properties along the optical path.

As a first step toward analyzing the temporal properties of flame radiation, the earlier stochastic approach of Jeng et al. (1984) was extended. This involved dividing the optical path into discrete eddies, each having uniform properties at any instant. The characteristic length of the eddies was assumed to be proportional to the local dissipation length scale, as follows:

$$L_e = C_e C_\mu^{3/4} k^{3/2} / \varepsilon \qquad (2.2)$$

where C_e is a constant of proportionality which was found by matching predictions and measurements. During earlier work, changes in time-averaged spectral radiation properties were not strongly affected by the magnitude of C_e, which was set equal to unity for lack of other information. The present study will show, however, that predictions of spectral radiation intensity fluctuations are strongly influenced by the selection of C_e.

A succession of eddies were assumed to cross the optical path at each eddy location, each eddy being present at the path for a characteristic eddy lifetime, t_e. Characteristic eddy lifetimes were estimated using Taylor's hypothesis, as follows:

$$t_e = L_e / u \qquad (2.3)$$

where u is the streamwise velocity for the eddy in question. Thus for each eddy of length L_e along the path, scalar properties were assumed to be uniform for a time t_e.

Eddy properties were randomly selected at the instant that the eddy reached the optical path. This involved making random selections of streamwise velocity and mixture fraction, satisfying the local probability density functions (PDF) of these variables. A Gaussian PDF, having a mean velocity and variance of $\tilde{u}$ and 2k/3, was assumed for the streamwise velocity. Time-averaged velocities should be used instead of the Favre-averaged velocities, however, time-averaged velocities are not accessible without substantially extending the present turbulence model – a step that was not taken until the need for extension has been established. Although time- and Favre-averaged mean velocities are similar, time-averaged velocity fluctuations are significantly larger (20-40 percent) than Favre-averaged velocity fluctuations in high-temperature portions of buoyant turbulent diffusion flames (Faeth and Samuelson, 1986); therefore, the present approximation introduces errors in the simulation of eddy velocities.

The time-averaged PDF of mixture fraction could be sampled directly, since it is available from the present turbulence closure. As noted earlier, a clipped Gaussian Favre-averaged PDF of mixture fraction was assumed during the structure analysis. The time-averaged PDF is then found as follows (Bilger, 1976):

$$\bar{P}(f) = \bar{\rho}\, \tilde{P}(f) / \rho \qquad (2.4)$$

The form of $\bar{P}(f)$ is not analytic, since $\tilde{P}(f)$ becomes skewed by the density weighting of equation (2.4).

The present simulation assumes that velocities and mixture fractions are statistically independent. This is not actually the case, also introducing errors in the simulation. Existing measurements in turbulent jet flames (Faeth and Samuelson, 1986; Stårner and Bilger, 1980) and buoyant plumes (Lai and Faeth, 1987) indicate that the cross-correlation between streamwise velocities and mixture fractions is roughly 0.5. This relationship could easily be incorporated into the simulation and it is planned to examine the need for such an extension in the future.

Given the mixture fraction at each instant and point along the optical path, from the stochastic simulation, the state relationships (Fig. 2) provide all scalar properties needed to solve the equation of radiative transfer along the path, using the narrow-band model. The results of this calculation provide the temporal variation of spectral radiation intensities for this path. All properties needed for the simulation are available from the solution for flame structure and the state relationships.

The temporal stochastic simulation begins by making random selections of velocities and mixture fractions for each eddy along the radiation path. Proceeding in time, the properties of each eddy are updated by new random selections after time intervals equal to the characteristic eddy lifetimes. The nature of the simulation for a particular eddy is illustrated in Fig. 3. The variation of f, u and t_e for the eddy are plotted as a function of time, yielding staircase waves with variable times of dwell, due to the variation of t_e from one eddy realization to the next. Given the variation of properties for each eddy along the radiation path, similar to the results illustrated in Fig. 3, spectral intensity calculations are carried out at convenient fixed intervals of time. During present work, the time intervals of the radiation calculations were chosen so that the predicted time variation of spectral radiation intensities could be analyzed by Fourier techniques to resolve the temporal power spectra up to the highest frequencies of interest.

2.4 Results and Discussion

2.4.1 Flame Structure

Structure measurements and predictions along the axis of the two flames are illustrated in Figs. 4 and 5. Recall that time-averaged velocities were measured while Favre-averages were predicted. The differences between these averages are less than 10 percent for mean velocities and generally less than 20 percent for velocity fluctuations (except near the flame tip where differences for velocity fluctuations approach 40 percent) with the Favre-averaged values being lower for present flame conditions (Stårner and Bilger, 1980; Faeth and Samuelson, 1986). The analysis only yields k; therefore, $\tilde{u}''$ has been estimated for plotting in the figures, assuming isotropic turbulence ($\widetilde{u''^2} = 2k/3$), which is consistent with the other turbulence model assumptions. If the usual levels of anisotropy observed along the axis of jets is assumed ($\widetilde{u''^2} = k$), predictions would be roughly 20 percent higher. Mean velocities along the axis are

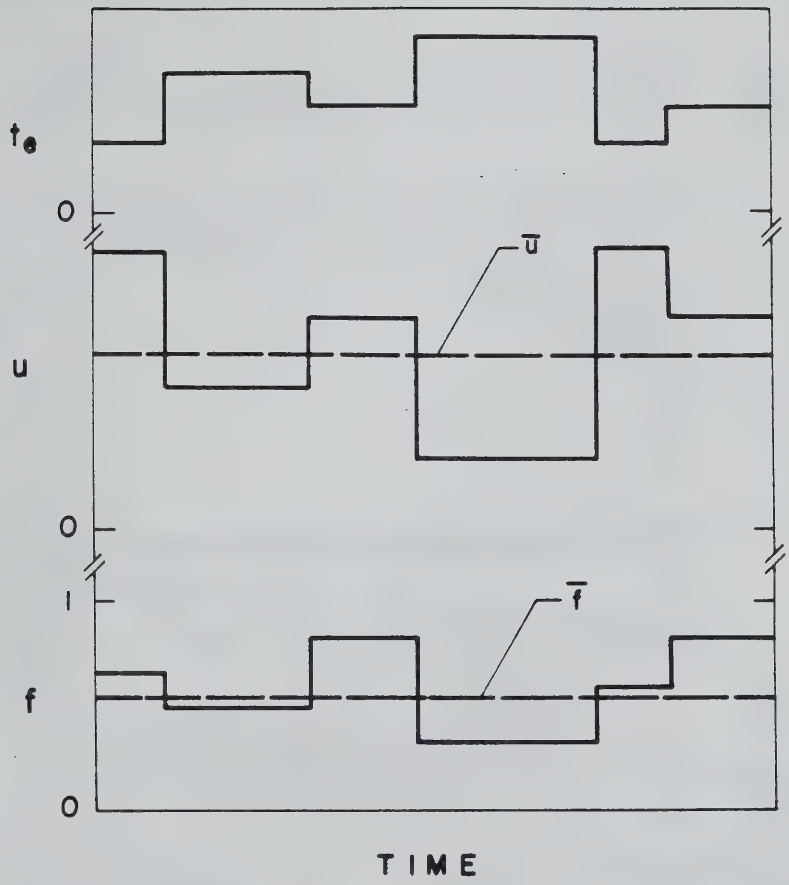

Figure 3. Sketch of temporal simulation of eddy properties.

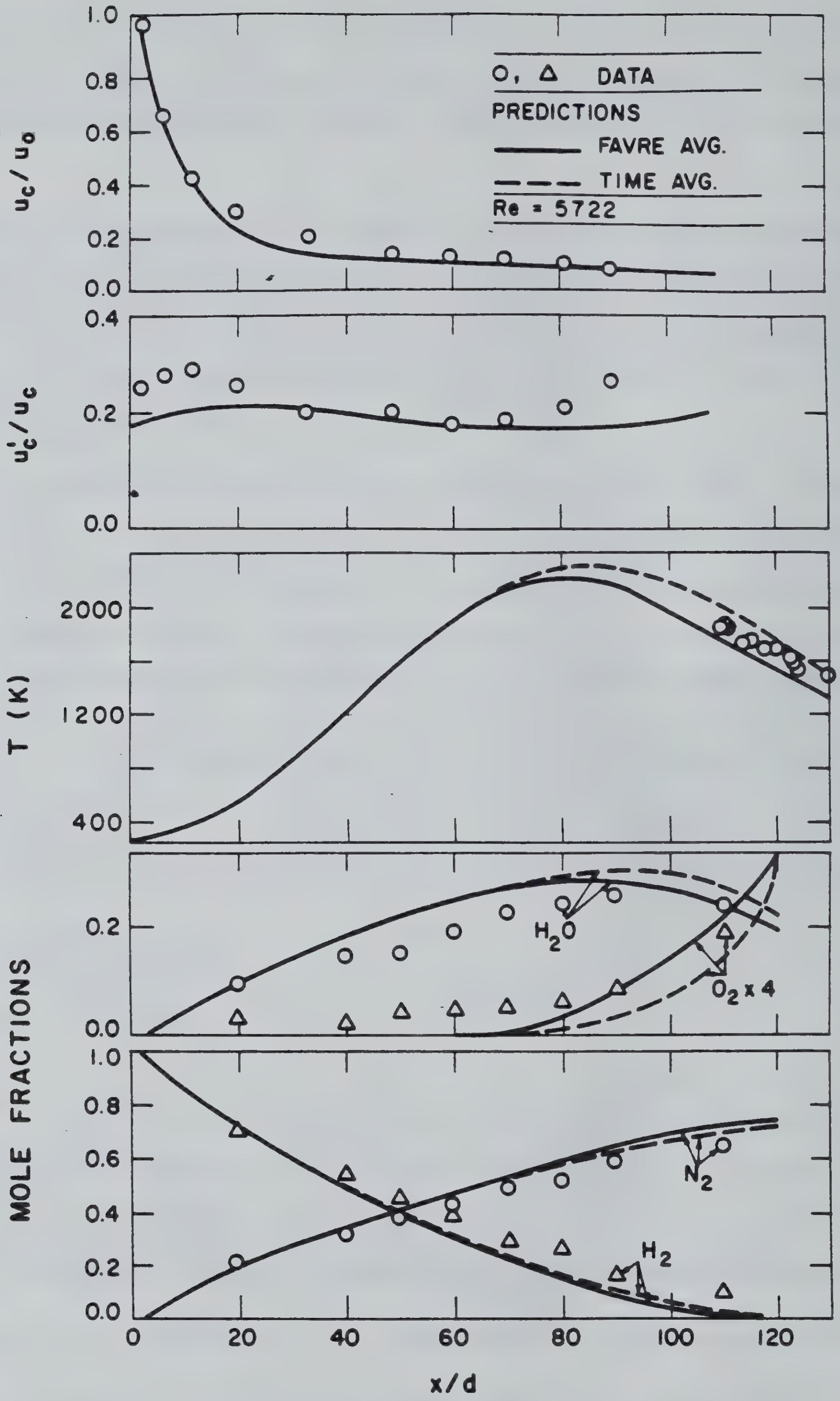

Figure 4. Properties along axis of hydrogen/air diffusion flame (Re = 5,720).

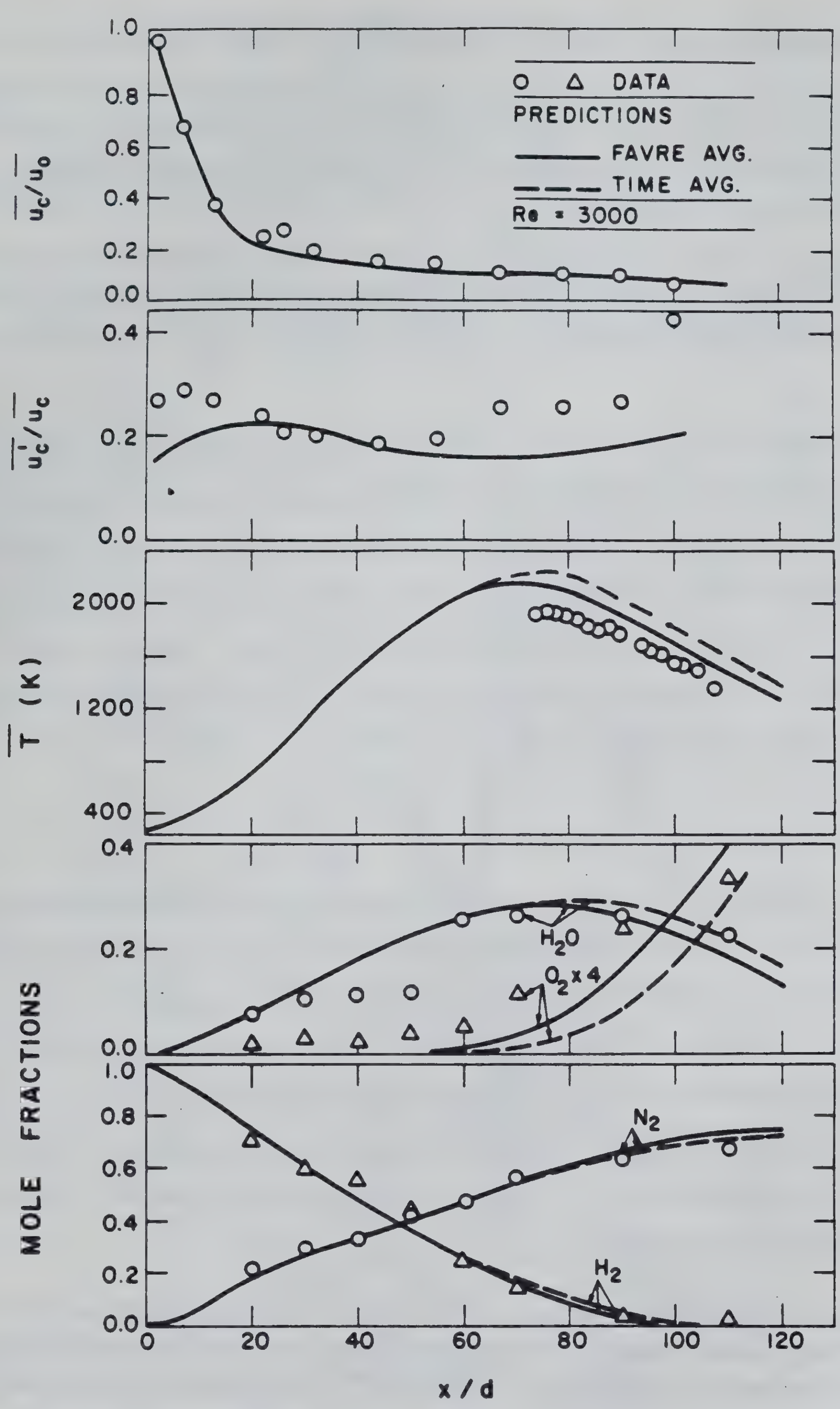

Figure 5. Properties along axis of hydrogen/air diffusion flame (Re = 3,000).

$(\widetilde{u''^2} = k)$, predictions would be roughly 20 percent higher. Mean velocities along the axis are predicted reasonably well. Predicted values of $\tilde{u}''_c$ are generally lower than the measured $\bar{u}'_e$ which is consistent with potential differences between the two averages and typical levels of anisotropy for this variable. Near and beyond the flame tip there is also additional production of turbulence due to turbulence/buoyancy interactions which have not been considered in the analysis (Jeng et al., 1982). This effect accounts for the rapid increase of $\bar{u}'_c$ for $x/d > 60$, which is not suggested by the predictions. The fact that the increase is greater for the lower Reynolds number flame (compare Figs. 4 and 5) supports the idea that the effect is due to buoyancy.

The analysis provides both time- and Favre-averaged scalar properties; therefore, predictions in Figs. 4 and 5 include both averages, since the degree of density weighting of the sampling measurements is unknown. For present conditions, however, differences between these averages is not large. Temperature measurements were not corrected for radiative heat losses and are 100-200 K too low in the hottest portions of the flow. Considering effects of radiation and uncertainties in the type of average measured, however, the comparison between predicted and measured temperatures is reasonably good. Predicted and measured concentrations are in reasonable agreement as well. The main discrepancy appears to be a tendency to slightly overestimate the rate of development of the higher Reynolds number flame, see Fig. 4, thus underestimating the flame length.

2.4.2 Mean Radiation Properties

The structure evaluation suggests that the present model provides reasonable predictions of mean properties for the flames under consideration; therefore, we turn to discussion of radiation properties. Measurements and predictions of spectral radiation intensities for the two flames are illustrated in Figs. 6 and 7. Measurements were undertaken for horizontal, radial paths at $x/d = 50$, 90 and 130. Results for $x/d = 130$ are not shown for the lower Reynolds number flame, since this position is well beyond the flame tip and spectral intensities were too low to be measured with acceptable levels of accuracy. Predictions using both the mean-property and stochastic methods are also shown on the figures. The stochastic predictions were based on $C_e = 1$, however, it was found that values of C_e in the range 1-6 yield essentially the same results.

The spectral radiation intensities in Figs. 6 and 7 are dominated by the 1380, 1870 and 2700 nm bands of water vapor. Intensities also increase gradually beyond 4000 nm, as the broad 6300 nm band of water vapor is approached. The stochastic method generally yields higher values of spectral radiation intensities than the mean property method, ca. 2:1. This suggests greater effects of turbulence/radiation interactions for hydrogen/air diffusion flames than either nonluminous carbon monoxide/air or methane/air diffusion flames, where

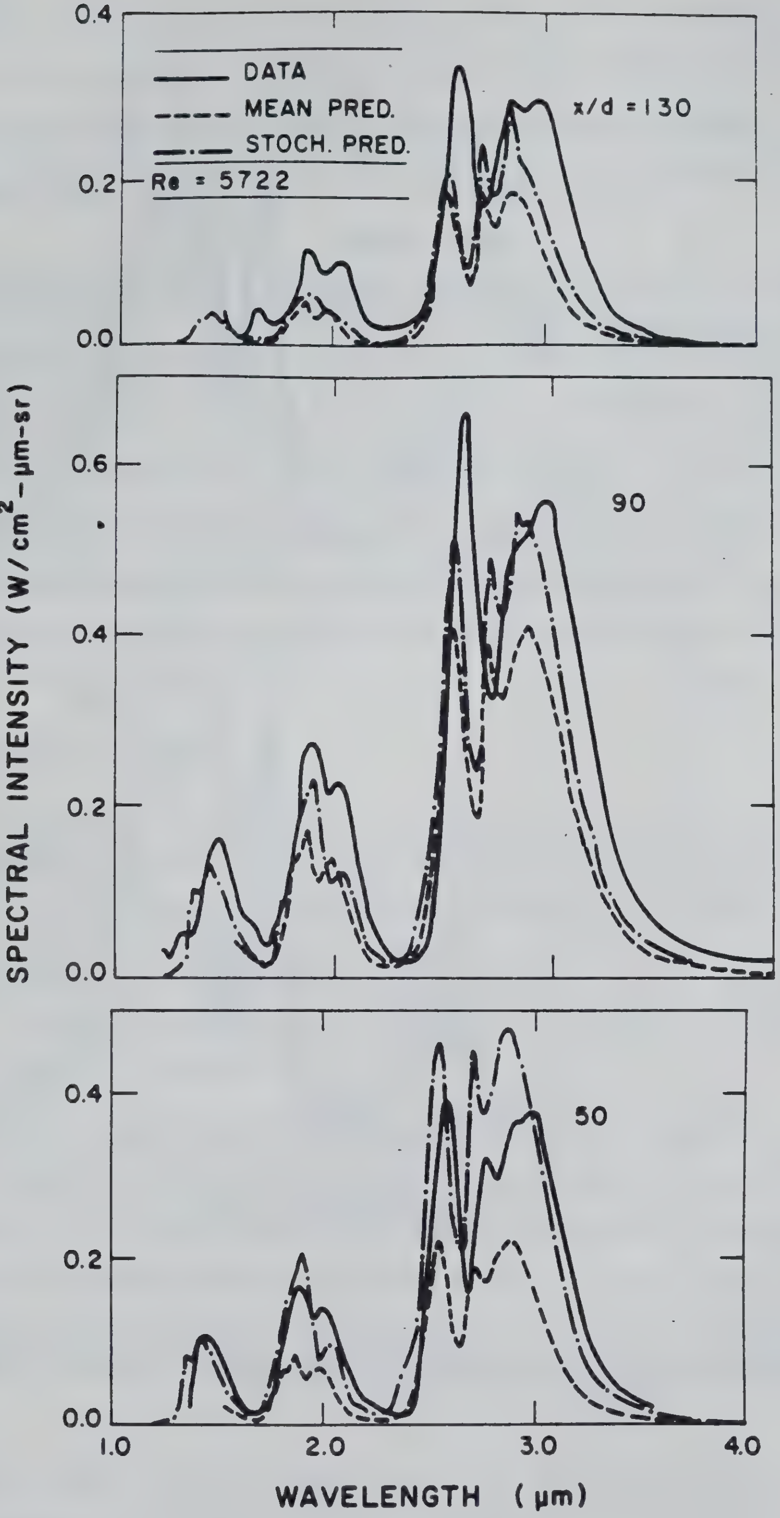

Figure 6. Mean spectral radiation intensities for hydrogen/ air diffusion flame (Re = 5,720).

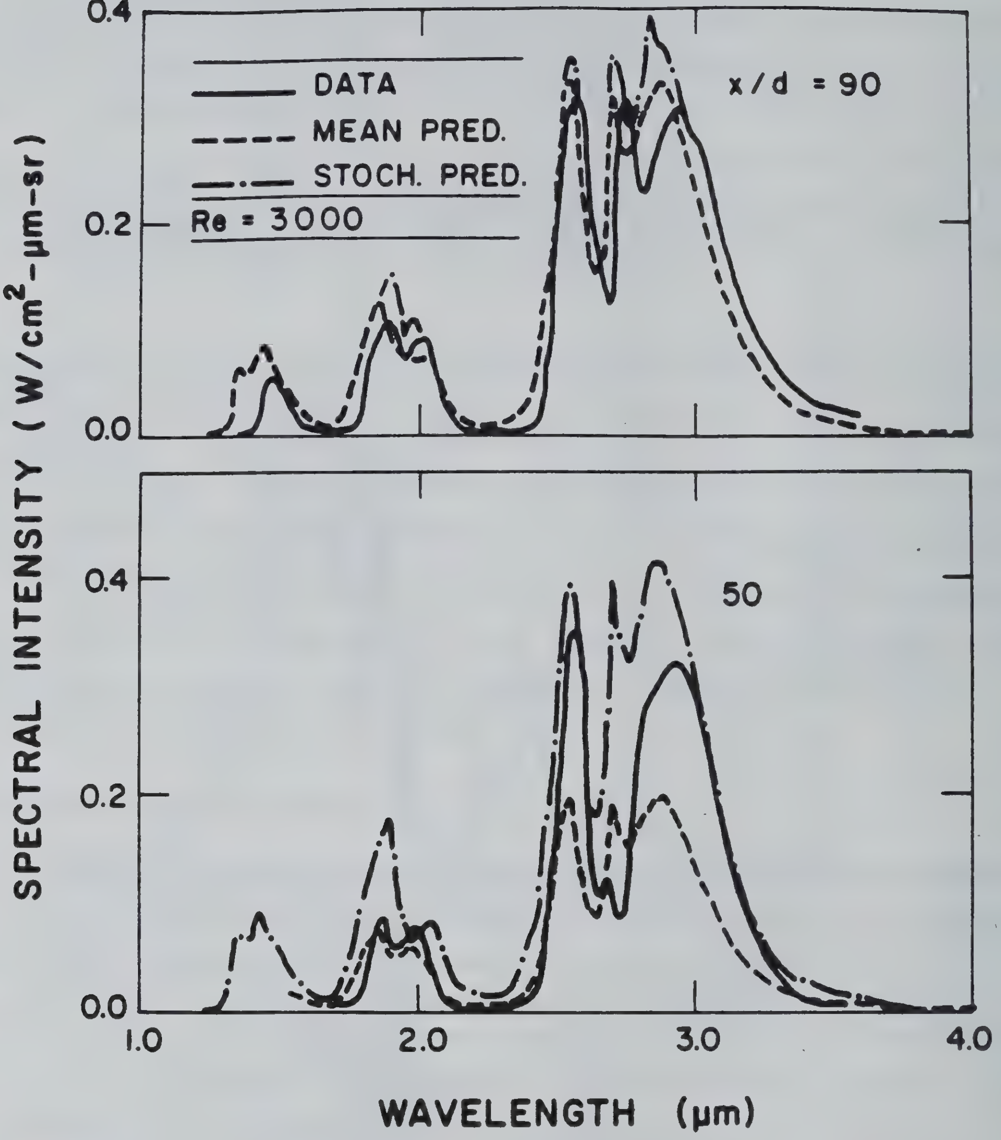

Figure 7. Mean spectral radiation intensities for hydrogen/air diffusion flame (Re = 3,000).

differences between the two methods were generally less than 30 percent (Jeng et al., 1984; Gore et al., 1987b). This behavior is caused by the rapid variation of radiation properties (viz., temperature and water vapor concentration) with mixture fraction near the stoichiometric condition for hydrogen/air diffusion flames. Thus predictions of the two methods tend to merge in the far field, however, this region also has relatively small radiation intensities for the present test conditions.

Measured spectral radiation intensities are generally between the two predictions with discrepancies on the order of 20 percent for each. This is very encouraging since both structure and radiation properties are predicted; and uncertainties in the narrow-band model, and also the structure model, are within the same range. An exception to this performance is the x/d = 130 position for the higher Reynolds number flame, see Fig. 7. This position is just beyond the flame tip, where spectral radiation intensities decrease very rapidly with increasing distance: present structure predictions tend to underestimate the length of this flame, as noted earlier, and this is largely responsible for the discrepancies seen in Fig. 7. Measured and predicted mean radiative heat fluxes were also predicted reasonably well for these flames, properly accounting for the position and direction of the heat flux sensor, and the Reynolds numbers of the flames (Gore et al., 1987c).

2.4.3 Radiation Fluctuations

The study of radiation fluctuations involved the same flames and radiation paths as the mean spectral radiation intensity measurements. However, these measurements were confined to a wavelength of 2520 nm (with a spectrometer slit width of 40 nm). This wavelength corresponds to a region of strong radiation emission in the 2700 nm band of water vapor, which is quite apparent in the flame spectra appearing in Figs. 6 and 7. Use of this strongly emitting region provided high signal-to-noise ratios for the measurements, simplifying determination of radiation fluctuations.

Before considering predictions and measurements, results of initial computations using the stochastic radiation analysis will be discussed. The objective of these calculations was to evaluate the sensitivity of predictions to the unknown parameter C_e, which appears in the expression for the characteristic eddy size (equation (2.2)). As noted earlier, changing C_e in the range 1-6 had essentially no effect on predictions of mean spectral radiation intensities using the stochastic method; therefore, only radiation fluctuations will be considered in the following.

Figure 8 is an illustration of the effect of $C_e = L_e / L_{eb}$ on predictions of root-mean-squared spectral radiation intensity fluctuations. Various points in both hydrogen/air diffusion flames are considered, for a wavelength of 2520 nm. The predictions show that radiation fluctuation levels progressively increase with increasing height above the burner exit. In

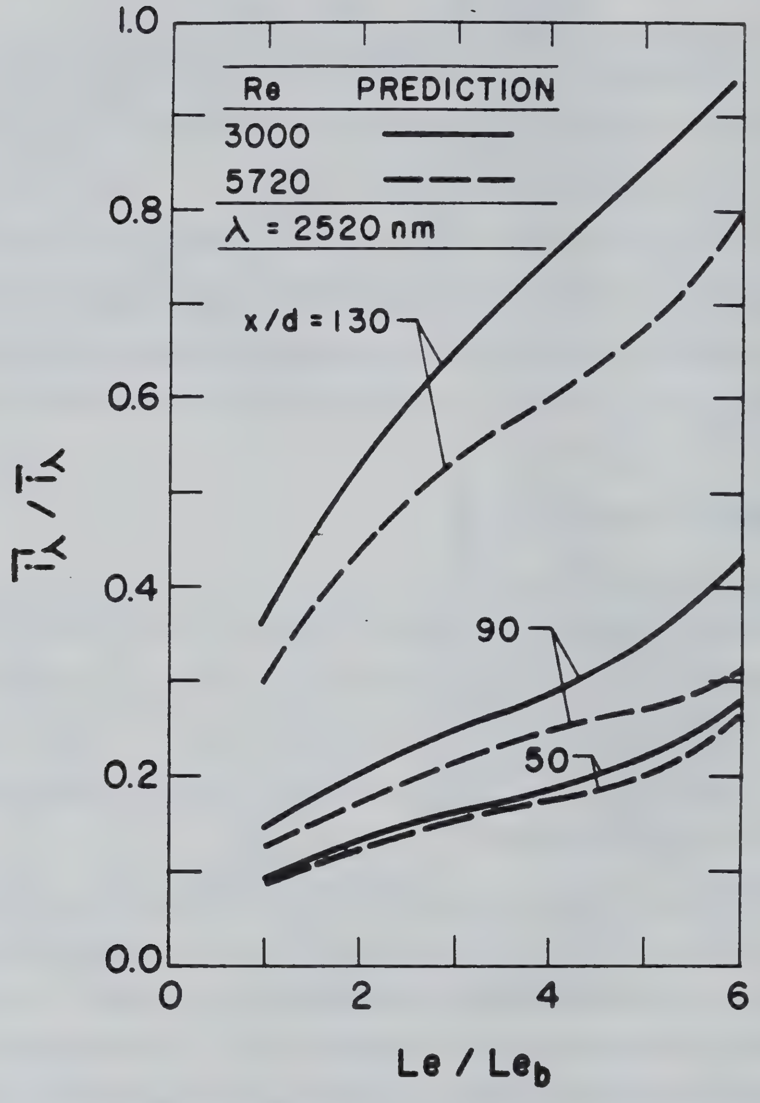

Figure 8. Effect of characteristic eddy size on spectral radiation intensity fluctuations.

addition, predicted radiation fluctuations increase strongly as $C_e = L_e / L_{eb}$ is increased, even though such changes have little effect on mean spectral radiation intensity predictions.

The selection of C_e also influences the temporal power spectra of spectral radiation intensity fluctuations. Define the Fourier transform of $i'_\lambda(t)$ over a finite interval, as follows:

$$I_\lambda(f) = \int_{-T}^{T} (i_\lambda'(t) / 2\pi) \exp(-2\pi i f t) dt \tag{2.5}$$

Then the power spectral density of the spectral radiation intensity fluctuations is given by

$$E(f) = \lim_{T \to \infty} (\pi \,|\, I_\lambda(f) \,|^2 / T) \tag{2.6}$$

More rigorously, the power spectral density of $i_\lambda'(t)$, which is a random function of time, is the Fourier transform of the autocorrelation of $i_\lambda'(t)$, as follows:

$$E(f) = \int_{-\infty}^{\infty} (R_\lambda(t)/2\pi) \exp(-2\pi\, i\, ft) dt \tag{2.7}$$

where the autocorrelation of $i_\lambda'(t)$ is defined as

$$R_\lambda(t) = \lim \; (1/2T) \int_{-T}^{T} i_\lambda'(\tau) i_\lambda'(\tau+t) d\tau \tag{2.8}$$

Predictions illustrating the effect of $C_e = L_e / L_{eb}$ on E(f) appear in Fig. 9. The normalized power spectrum has been plotted as a function of normalized frequency (where $\bar{u}_c/x$ has been taken to be the characteristic frequency at a particular height above the burner). Results at x/d = 50 for the low Reynolds number hydrogen/air diffusion flame are shown, however, findings for other flame conditions examined during this investigation were similar. The power spectra have largest amplitudes at low frequencies, typical of most phenomena associated with turbulence. The spectra begin to decrease sharply near a normalized break frequency of unity, suggesting that the frequency scaling used in Fig. 9 is realistic. There is a high-frequency cut-off at frequencies roughly an order of magnitude larger. The selection of $C_e = L_e / L_{eb}$ is seen to have a significant effect on the spectrum, with lower values of C_e causing an increase in the high-frequency cut-off frequencies. This is expected since smaller values of C_e imply smaller characteristic eddies which have shorter characteristic residence times, introducing higher frequencies into the stochastic simulation. Another property of the simulation is that a peak in the spectrum appears, near $fx / \bar{u}_c$ of unity, as $C_e = L_e / L_{eb}$ becomes larger. This is particularly evident for the low Reynolds number near-injector

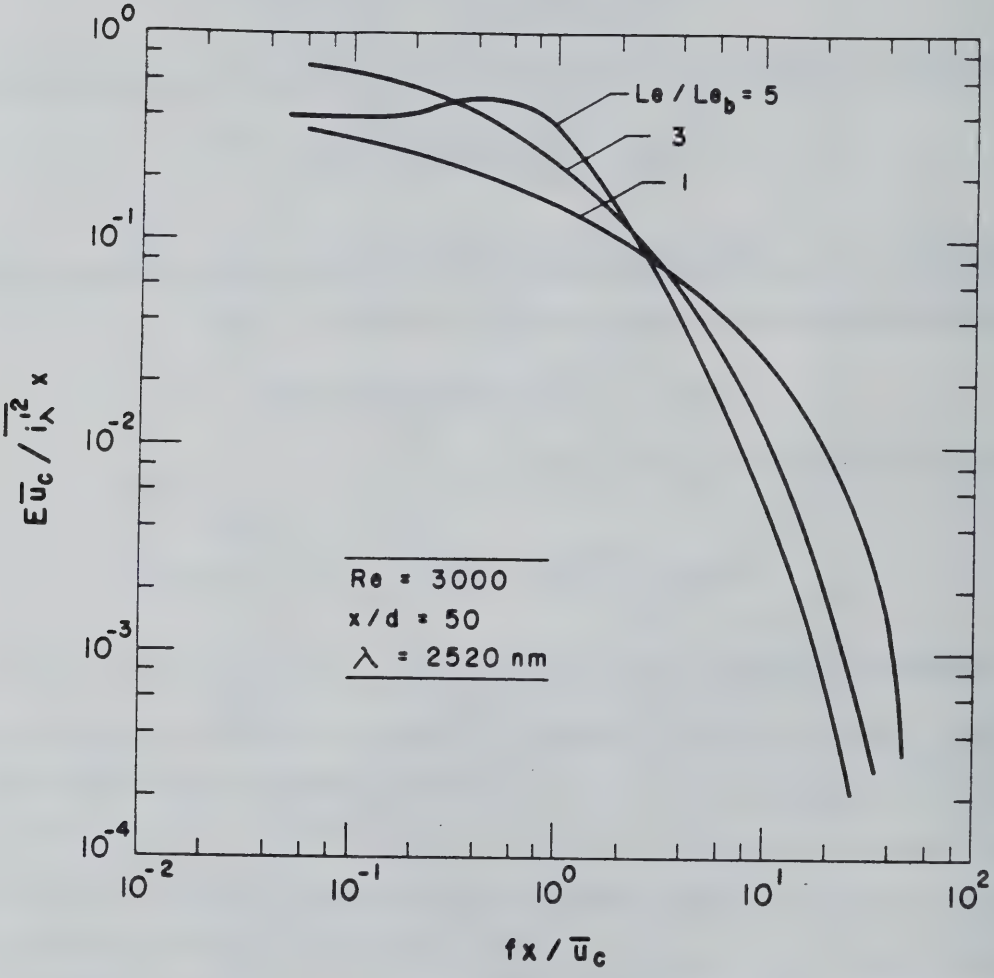

Figure 9. Effect of characteristic eddy size on the power spectrum of spectral radiation intensity fluctuations (Re = 3,000, x/d = 50).

condition illustrated in Fig. 9. The behavior is due to the presence of fewer eddies in the optical path, which tends to concentrate the flame sheets in single eddies positioned symmetrically with respect to the axis, which magnifies signal energy at the characteristic frequencies of these eddies. With more eddies in the optical path (lower L_e / L_{eb}), the flame sheets shift over a wider range of eddies, and the greater variation of characteristic eddy frequencies broadens and eventually eliminates the peak. This effect is most evident at low Reynolds numbers, since concentration fluctuation intensities are relatively small at such conditions, tending to isolate the flame sheets to single eddies when there are only a few eddies in the optical path.

The selection of C_e has a strong influence on predictions of radiation fluctuations. Therefore, present measurements were used to optimize its value. Since current data is limited, this selection was limited to the nearest integer, thus, $C_e = 5$ was chosen to provide the best overall match between predictions and measurements.

For present conditions, $C_e = 5$ implies roughly 6 eddies within the flame for the stochastic simulation of a horizontal optical path through the axis, relatively independent of height above the burner. This number is quite plausible, since it corresponds to the number of integral concentration length scales typically observed across the diameter of turbulent round jets (Becker et al., 1967; Shaughnessy and Morton, 1977). Due to the integral nature of spectral radiation intensities along a path, high frequency effects tend to be integrated out, thus the large eddy structures in the flow should dominate radiation properties – which is consistent with present observations.

Measured and predicted mean and fluctuating spectral radiation intensities are summarized in Tables 2 and 3. Results are considered for x/d = 50, 90 and 130 for both flames, at a wavelength of 2520 nm. Measurements include optical path diameters of 5 and 10 mm, however, differences between the two conditions are comparable to experimental uncertainties and do not differ in any consistent pattern. Predictions were obtained for $C_e = 5$, and represent the limit of an infinitely-small diameter path.

The intensity of measured spectral radiation fluctuations in Table 3 is never less than 20 percent and reaches values in excess of 100 percent beyond the flame tip. This provides clear experimental evidence of strong effects of turbulence/radiation interactions in these flames. The comparison between predictions and measurements in Tables 2 and 3 is quite encouraging. The trends of both mean and fluctuating spectral radiation intensities are predicted quite well, both with respect to position and flame Reynolds number. The absolute agreement between predictions and measurements is also reasonably good: average differences between predictions and measurements are roughly 30 percent for mean intensities, and roughly 25 percent for intensity fluctuations. Greatest errors are observed at x/d = 130 for the highest Reynolds number flame. As noted in connection with Fig. 6, radiation predictions are very sensitive to predictions of mixing near x/d = 130 for this flame, thus, deficiencies of the structure analysis are probably largely responsible for the poorer performance at this position. Overall, in view of anticipated uncertainties in the structural analysis, the narrow-band radiation model, and certainly the present crude stochastic simulation of radiation properties, the comparison between predictions and measurements in Tables 2 and 3 is about as good as could be expected.

Table 2. Mean Spectral Radiation Intensities (W/cm^2 sr μm) for Hydrogen/Air Diffusion Flames[a]

x/d	Path Diameter (mm)		
	10	5	Predicted[b]
Re = 3000:			
50	0.39	0.35	0.41
90	0.37	0.39	0.37
130	0.067	0.10	0.057
Re = 5720:			
50	0.39	0.35	0.45
90	0.60	0.51	0.45
130	0.39	0.33	0.11

[a] At a wavelength of 2520 nm and a resolution (at half peak transmission) of 40 nm.

[b] Infinitely small path diameter for $C_e = 5$.

Table 3. Intensity of Spectral Radiation Intensity Fluctuations (Percent) for Hydrogen/Air Diffusion Flames[a]

x/d	Path Diameter (mm)		
	10	5	Predicted[b]
Re = 3000:			
50	24	27	23
90	46	36	35
130	107	80	91
Re = 5720:			
50	21	29	21
90	23	25	27
130	45	39	67

[a] At a wavelength of 2520 nm and a resolution (at the half-peak transmission) of 40 nm.

[b] Infinitely-small path diameter for $C_e = 5$.

Predicted and measured probability density functions of i_λ are illustrated in Figs. 10 and 11, considering the same flame Reynolds numbers and positions as before. Measurements are provided for both optical path diameters, however, there is little difference between the two. Predictions represent an infinitely-small diameter optical path.

The PDF's in Figs. 10 and 11 are skewed, which is particularly evident for the predictions. For positions below the flame tip (x/d = 50 and 90 for Re = 5720 and x/d = 50 for Re = 3000), the maximum of the PDF's is generally at values of i_λ greater than the time average. In this region, the stoichiometric condition (flame sheet) is present, which yields the maximum contribution to the spectral radiation intensity. Since all other mixture fractions yield lower spectral radiation intensities, the PDF must be biased toward values of i_λ greater than the

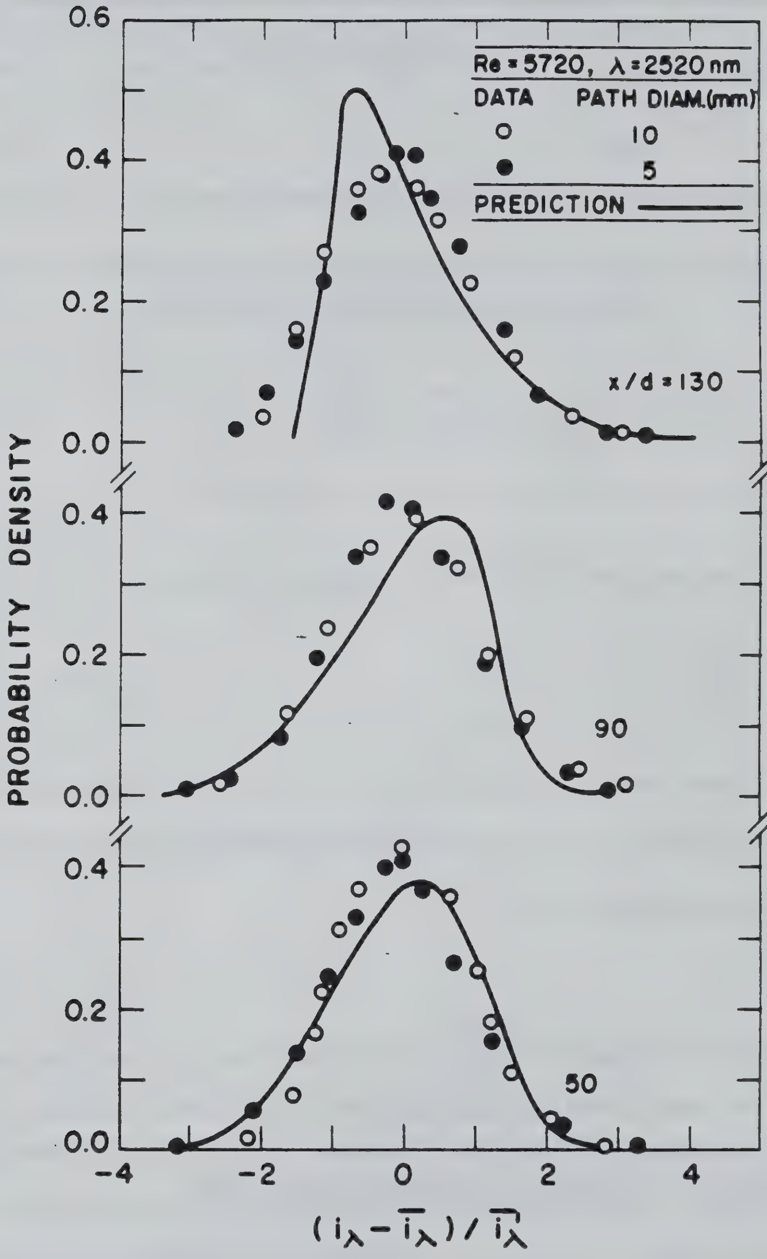

Figure 10. Probability density of normalized spectral radiation intensities for hydrogen/air diffusion flame (Re = 5,720).

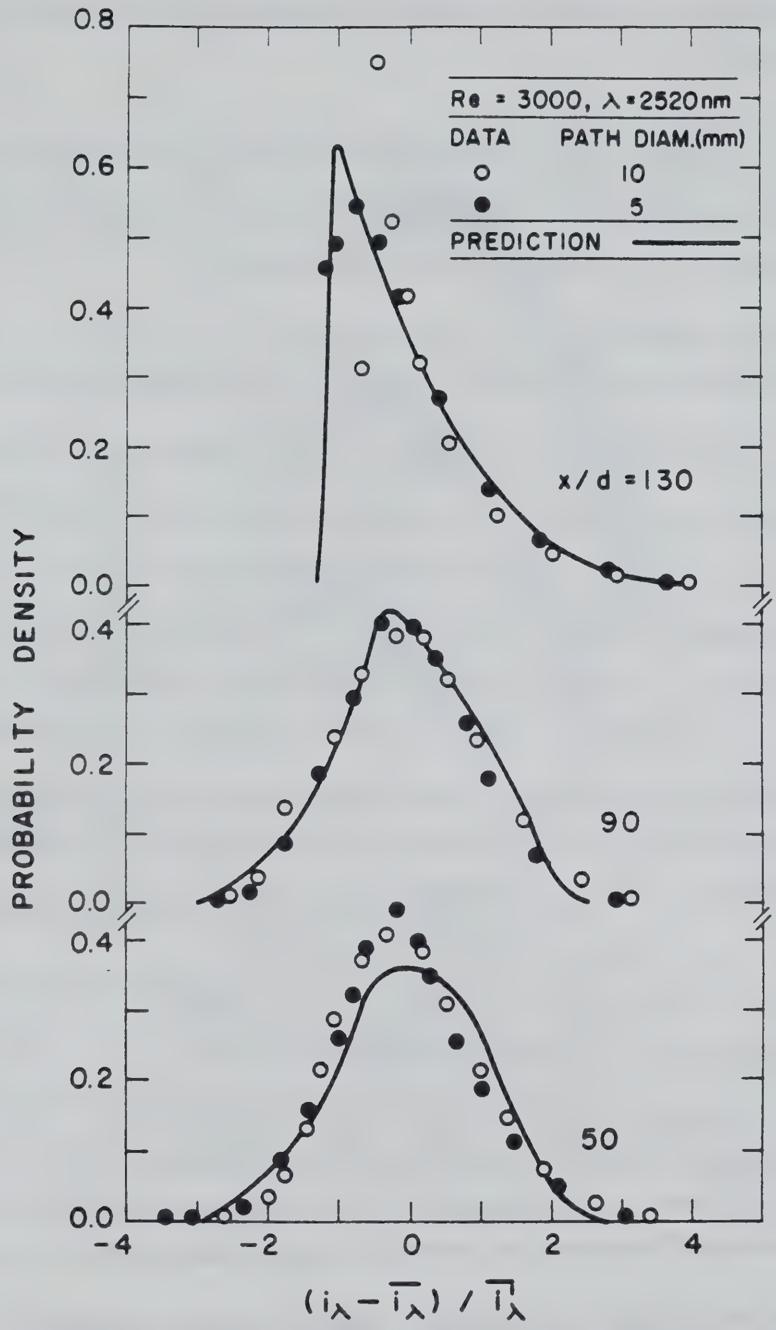

Figure 11. Probability density of normalized spectral radiation intensities for hydrogen/air diffusion flame (Re = 3,000).

time average to compensate for this physical limit. Conversely, beyond the flame tip (x/d = 130 for Re = 5720 and x/d = 90 and 130 for Re = 3000) the flame sheet is rarely present. However, the minimum contribution to the spectral radiation intensity comes from the ambient air. Thus, as intermittency increases, the most probable condition of the PDF moves below the time-averaged value of i_λ.

The predictions represent the measured PDF's reasonably well including effects causing skewness. Once again, the largest discrepancies between predictions and measurements are observed for the highest Reynolds number flame at x/d = 130 (see Fig. 10) where difficulties in the structure analysis are probably the source of the problem.

Predicted and measured power spectral densities of fluctuations of spectral radiation intensities are illustrated in Figs. 12 and 13. Both the power spectra and the frequencies are normalized by the characteristic frequency, $\bar{u}_c/x$, at each height above the burner. Measurements are provided for both optical path diameters. In contrast to other fluctuating radiation properties, power spectra are influenced appreciably by the diameter of the radiation path. The smaller diameter path has greater signal energy at high frequencies, which is expected since larger path diameters tend to average out high frequency variations in the spectral intensity. Differences in the spectra for the two optical path diameters become smaller with increasing height above the burner. This is also expected since integral scales increase with height above the burner so that both paths eventually become small in comparison to characteristic eddy size.

The power spectra for the high Reynolds number flame (Fig. 12) decrease monotonically from the energy-containing portion of the spectra at low frequencies. The decrease in the spectra begins at roughly $f\bar{u}_c/x = 0.2$ at x/d = 50, with this break frequency appearing near $f\bar{u}_c/x = 1.0$ at x/d = 90 and 130. That the normalized break frequency approaches unity for large x/d is probably fortuitous, however, the upward shift of the normalized break frequency near the burner can be explained by considering the flame structure. In all regions, the highest temperature portion of the flow contributes most to the spectral radiation intensities. For low positions, there are two high-temperature regions (the flame sheets) in the optical path, both of which are near the edge of the flow where local velocities are much smaller than at the axis. Integral length scales, however, are relatively constant across the width of the flow. Thus, the most important radiation fluctuations are controlled by eddy passing times, L_e/u, that are longer than passing times near the axis. As a result, a break frequency less than $\bar{u}_c/x$ is expected. Near the flame tip (x/d ca. 90-110 for the present flames) and beyond, however, the maximum contribution to radiation fluctuations is associated with the axis, where velocities are highest, and a higher normalized break frequency, $fx/\bar{u}_c$, is expected.

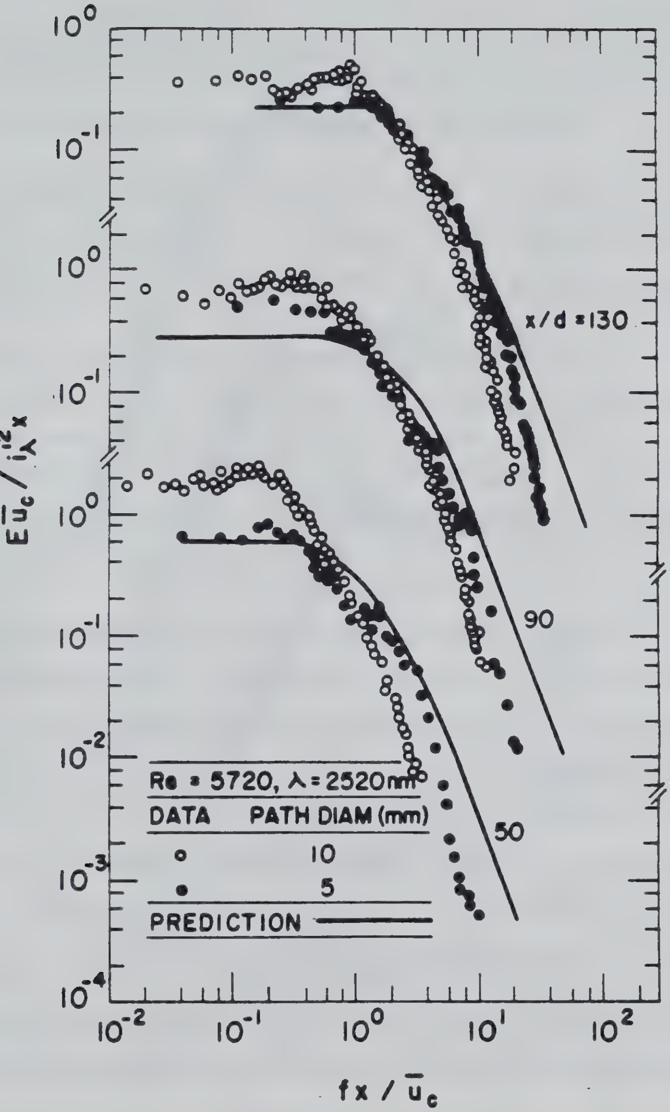

Figure 12. Power spectra of spectral radiation intensity fluctuations for hydrogen/air diffusion flame (Re = 5,720).

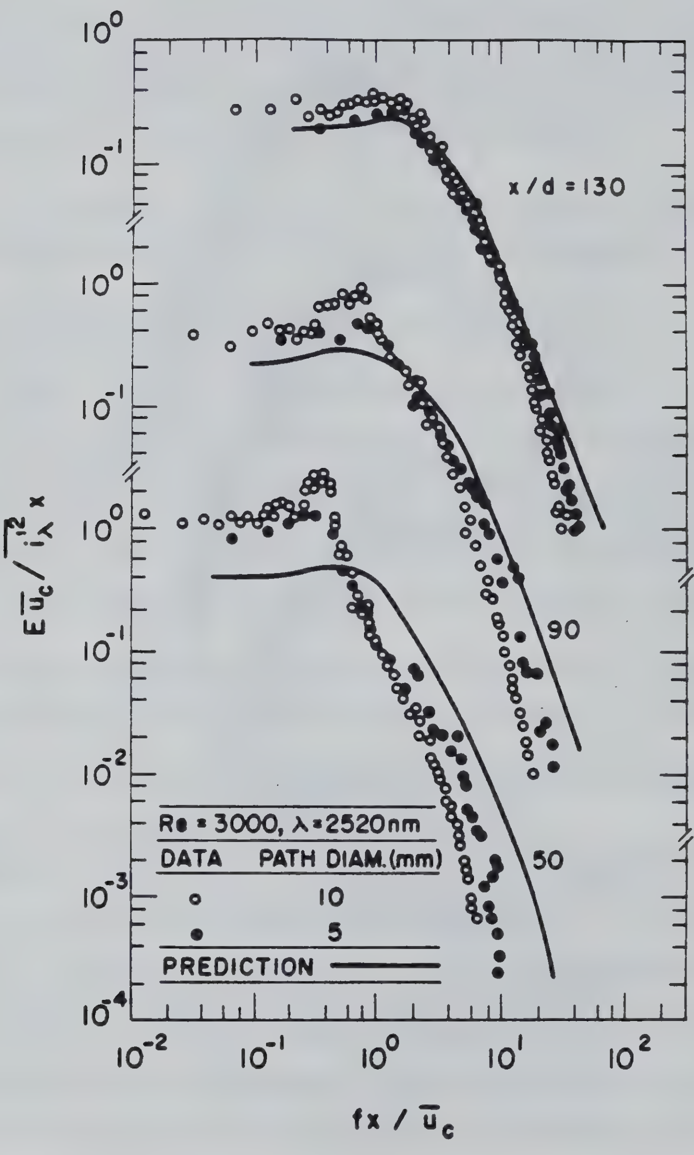

Figure 13. Power spectra of spectral radiation intensity fluctuations for hydrogen/air diffusion flame (Re = 3,000).

The measured spectra of the low Reynolds number flame are similar to the high Reynolds number flame (cf. Figs. 12 and 13), except that a peak near the break frequency appears in the spectra – particularly for the lowest position. The predictions also exhibit a slight peak, but not as large a peak as the measurements. The reasons for the predicted behavior were discussed earlier: namely, lower concentration fluctuation intensities when the Reynolds number is lower tends to confine signal energy to eddies near the mean stoichiometric condition. The larger peak of the measurements can probably be attributed to the regular formation and release of large eddy structures which are often observed near the source of buoyant flows. The peaks are larger for the larger diameter optical path: this also suggests that phenomena causing the peak have relatively large spatial coherence.

The power spectra in Figs. 12 and 13 exhibit a region of regular decay with increasing frequency, just beyond the break frequency. The region is reminiscent of the inertial range of the spectra of other turbulence properties, however, the rate of decay is unusually large – approaching $f^{-5/2}$. This behavior is difficult to interpret, since the temporal variation of properties along the initial optical path are involved. The tendency for effects of scalar fluctuations on radiation properties to integrate out after ten or so wavelengths may be a factor in the relatively fast truncation of high-frequency phenomena. At the highest frequencies, the rate of decay of the power spectra becomes even more rapid, suggesting approach to a high-frequency cut-off at small scales. However, present signal-to-noise ratios were not high enough to accurately define the cut-off frequencies.

The comparison between predicted and measured power spectra in Figs. 12 and 13 is very encouraging, particularly since C_e was only chosen to optimize predictions of rms radiation fluctuations. The agreement between predictions and measurements for an optical path diameter of 5 mm is best, since the predictions are most appropriate for path diameters which are much smaller than characteristic eddy sizes. Break frequencies, and their shift toward higher values of $fx/\bar{u}_c$ with increasing x/d, are also predicted reasonably well. An exception is x/d = 50 for Re = 3000, which exhibits a peak in the measured power spectra that is only slightly reflected by the predictions. As noted earlier, the presence of the peak may be due to large scale unsteadiness, which cannot be represented by the present turbulence model. The rate of decay of the spectra in the initial region is also predicted reasonably well, although the high frequency cut-off is less apparent in the predictions than the measurements.

2.5 Summary

2.5.1 Conclusions

This is a report of progress on a continuing investigation. The main conclusions that can be drawn from results thus far are as follows:

1. Effects of turbulence/radiation interactions are very important for hydrogen/air diffusion flames, with stochastic predictions of mean spectral radiation intensities being generally two times larger than predictions based on mean scalar properties.

2. Measurements of the intensity of spectral radiation intensity fluctuations provided direct experimental evidence of the importance of turbulence/radiation interactions in hydrogen/air flames. For present test conditions, which were confined to optical paths through the flame axis, these intensities were in the range 20-110 percent.

3. Predictions of mean spectral radiation intensities were relatively independent of the characteristic eddy size used in the stochastic simulation, however, the properties of radiation fluctuations strongly depend on this parameter. The best match between predictions and measurements was achieved using characteristic eddy sizes that were 5 times the dissipation length scale given by the present turbulence model. This characteristic eddy size is comparable to the integral scales of the present flows, suggesting that the largest turbulent structures in the flame exert the greatest influence on radiation fluctuations.

4. The power spectra of radiation fluctuations exhibit an energy-containing range for $fx/\bar{u}_c$ less than roughly unity, with somewhat lower break frequencies observed before the flame tip. At frequencies higher than the break frequency, the spectra exhibit an inertial range and decay according to $f^{-5/2}$. The spectra also probably have a high-frequency cut-off, however, present signal-to-noise ratios were not large enough to resolve the cut-off.

5. The present stochastic radiation analysis gave encouraging predictions of mean and fluctuating radiation properties. Differences between predicted and measured mean and fluctuating spectral radiation intensities averaged roughly 30 percent, with generally similar agreement for the properties of the power spectra of i_λ.

2.5.2 Plans

Although the present stochastic analysis gave encouraging results, is is clearly ad hoc. The highest priority at this point is to convert this methodology to a more rigorous method. This will be done by formal time series simulation methods, following Box and Jenkins (1976). For present purposes, the combined temporal and spatial correlations of mixture fraction must actually be satisfied, which has no counterpart in time-series simulation, thus, existing methods will have to be extended. Using this technique, simulating the temporal properties of mixture fraction implies accepting the laminar flamelet approximation for turbulent flames, however, all results to date suggest that this approximation is reasonably satisfactory for buoyant diffusion flames.

Work thus far has established the importance of turbulence/radiation interactions and the importance of mixture fractions in establishing these properties. Little information is available concerning the statistical properties of mixture fractions in turbulent flames; therefore, emphasis will be placed on measuring these properties as well as mean and fluctuating radiation properties in nonluminous flames.

Convincing evaluation of stochastic methods for treating radiation fluctuations for nonluminous turbulent diffusion flames requires consideration of other reactant systems than hydrogen/air. Thus, subsequent work will also consider carbon monoxide/air and methane/air diffusion flames emphasizing conditions treated in the past (Gore et al., 1987b, Jeng et al., 1982, 1984), in order to avoid extensive measurements to define the flame structure.

3. LUMINOUS FLAMES

3.1 Introduction

Most unwanted fires involve soot-containing luminous flames, which radiate more strongly than nonluminous flames due to continuum radiation from soot. In order to better understand radiation phenomena associated with soot, studies of the structure and radiation properties of luminous turbulent ethylene/air and acetylene/air diffusion flames were recently completed in this laboratory (Gore et al., 1987a,b). However, these studies emphasized radiation properties, leaving uncertainties concerning scalar structure, particularly in the overfire (lean) region. The objective of the present investigation was to consider the scalar structure of the overfire region of the same flames, with particular emphasis on the scalar properties needed for analysis of flame radiation.

Predictions of flame radiation require information concerning the concentrations of major gas species and the properties of soot (Gore et al., 1987a,b). Soot particles in flames generally have diameters smaller than 100 nm, while infrared radiation having wavelengths greater than 1000 nm is most important; therefore, the Rayleigh limit of small particles is generally acceptable for estimating the spectral absorption coefficients of soot, and scattering can be ignored (Tien and Lee, 1982). As a result, the only soot properties needed for radiation analysis are the refractive indices and volume fractions of soot. There is some controversy concerning the refractive indices of soot; however, they are relatively independent of the original fuel and estimates are available in the literature (Tien and Lee, 1982). Thus, soot volume fractions are the soot property that must be found from predictions of flame structure, in order to analyze radiation from luminous flames.

As we have seen, the laminar flamelet concept for diffusion flames, proposed by Bilger (1977) and Liew et al. (1981), has significant potential for simplifying estimation of scalar properties needed for radiation analysis of turbulent diffusion flames. The concept is based on the observation that the concentrations of major gas species are nearly universal functions of mixture fraction (the fraction of mass which originated from the burner) within laminar flames, relatively independent of position and the degree of local flame stretch (Bilger, 1977).[1] The concept is applied to turbulent flames by assuming that they correspond to wrinkled laminar flames having the same universal correlations between scalar properties and mixture fraction. The latter can be found by analysis of turbulent mixing; therefore, the laminar flamelet concept replaces the problem of complex flame chemistry in a turbulent environment by routine measurements in laminar flames.

---

[1] Exceptions to these correlations are observed in regions of high flame stretch, associated with points of flame attachment and extinction (Liew et al., 1981); however, such regions are generally only a small fraction of the entire flow field. Minor gas species, like radicals and pollutants, exhibit larger regions where universality is lost (Faeth and Samuelsen, 1986); however, except for soot, these substances generally have little effect on flame radiation.

Correlations between scalar properties and mixture fraction have come to be called "state relationships" (Faeth and Samuelsen, 1986). State relationships for the concentration of major gas species have been measured for a variety of fuels burning in air at normal temperatures and pressures, as follows: hydrogen (Bilger, 1977; Gore et al., 1987c), carbon monoxide (Gore et al., 1987b), methane (Bilger, 1977; Jeng and Faeth, 1984a), propane (Jeng and Faeth, 1984b), n-heptane (Bilger, 1977), ethylene (Gore and Faeth, 1987a) and acetylene (Gore and Faeth, 1987b). Local thermodynamic equilibrium is generally observed for lean conditions; however, hydrocarbon fuels depart significantly from equilibrium at fuel-rich conditions, due to slow chemical processes associated with fuel decomposition and soot formation. Nevertheless, a quasi-equilibrium is reached at fuel-rich conditions for these materials as well, yielding universal correlations of major gas species concentrations as a function of mixture fraction, required by the laminar flamelet concept.

If the laminar flamelet concept can be extended to soot volume fractions, it would vastly simplify estimation of scalar properties needed for radiation analysis of luminous flames. Existing measurements by Kent and Bastin (1984), Kent (1987) and Becker and Liang (1983), for turbulent soot-containing flames, provide some evidence that this potential may exist for a useful range of flame conditions – particularly for the buoyant turbulent flames typical of unwanted fires. Kent and Bastin (1984) used laser extinction measurements to study effects of residence time on soot concentrations within acetylene/air diffusion flames. They observed that soot concentrations become relatively independent of residence time, for sufficiently long residence times, suggesting that a quasi-equilibrium condition was being approached for soot properties. Subsequently, Kent (1987) determined that characteristic soot volume fractions (a parameter related to the maximum soot volume fractions in a turbulent flame), were relatively independent of residence time for sufficiently long residence times and were related to the same parameter found in laminar flames for a variety of fuels. Becker and Liang (1983) studied turbulent sooting flames for a wide range of conditions. They found that the mass percentage of fuel carbon which was converted to soot and emitted from the flames, defined as the soot generation efficiency (Newman and Steciak, 1987), also became relatively independent of flame conditions for sufficiently long residence times. All these observations suggest a potential for universal soot volume state relationships, particularly at sufficiently-long residence times.

Soot volume fraction state relationships were examined during earlier studies of ethylene and acetylene flames in this laboratory (Gore and Faeth, 1987a,b). Measurements in laminar jet flames showed that soot volume fractions were only appreciable for a relatively narrow range of mixture fractions in the fuel-rich region (soot spikes) near the stoichiometric condition. State relationships for soot volume fractions were found within the soot spikes; however, the correlations were inferior to the state relationships for major gas species. This was attributed to effects of finite-rate chemistry, laminar hydrodynamics associated with the small diffusivities of soot particles, and effects of thermophoresis of soot particles (Santoro et al., 1983b; Pagni and Okoh, 1985). Nevertheless, subsequent use of these soot volume fraction state relationships for predictions of radiation emission and absorption in turbulent flames yielded encouraging agreement with measurements, suggesting that they were at least sufficiently universal to be useful for analyzing flame radiation properties (Gore and Faeth, 1987a,b). The situation is helped by the relative insensitivity of continuum-radiation predictions to estimates of soot volume fractions in comparison to other properties, e.g., sensitivity studies showed that a five percent increase in soot volume fractions increased spectral intensities in the continuum less than three percent, while a similar increase in temperature yielded intensity increases of 30-50 percent (Gore and Faeth, 1987b).

The earlier studies of turbulent ethylene and acetylene flames (Gore and Faeth, 1987a,b) highlight the importance of the presence of soot in the overfire region. In particular, the turbulent flames emitted soot, and emission and extinction of radiation by soot in the overfire region was significant. In order to treat effects of soot on the radiation properties of the overfire region, the soot volume fraction state relationships were extended into the lean region. This was done by selecting constant volumetric soot generation coefficients[2] for each fuel. This is equivalent to assuming that the soot volume fraction and the mixture fraction when soot oxidation ceases (near stoichiometric conditions) are the same for all paths through the flame, and that subsequently soot only passively mixes in the overfire region. The selections of volumetric soot generation efficiencies were optimized to some extent by extinction measurements in the overfire region. This approach yielded encouraging radiation predictions for the turbulent flames, however, a more direct evaluation of the lean portions of the soot volume fraction state relationships would be desirable. Finally, additional assessment of scalar structure predictions is needed, in order to evaluate effects of errors in the structure analysis on the radiation predictions.

The present phase of the investigation seeks to supply information on soot volume fractions and scalar structure in the overfire region of the turbulent ethylene and acetylene flames studies earlier (Gore and Faeth, 1987a,b). Measurements were made of the mean concentrations of major gas species and soot volume fractions. Predictions of these properties, using methods developed earlier (Gore and Faeth, 1987a,b), were evaluated using the new measurements. Soot volume fraction state relationships for the overfire region and soot generation efficiencies were also studied by directly correlating measured soot volume fractions and mixture fractions.

---

[2] The volumetric soot generation coefficient is defined as the volume of soot emitted from the flame per unit mass of fuel reacted.

This part of the report begins with a brief description of experimental and theoretical methods. This is followed by discussion of the findings for the turbulent acetylene and ethylene flames, in turn, considering: predicted and measured properties along the axis, mixture fractions, species concentrations, soot volume fractions, and the correlation of soot volume fraction state relationships in the overfire region. Soot generation efficiencies of the present flames, and their comparison with the measurements of others, are then considered. The report ends with a summary of conclusions obtained from results to date, and plans for research.

3.2 Experimental Methods

3.2.1 Apparatus

The test arrangement was the same as the earlier studies of turbulent ethylene and acetylene flames (Gore and Faeth, 1987a,b). The fuels were injected vertically upward from a water-cooled burner having an exit diameter of 5 mm. The flames were burned within a screened enclosure, in order to reduce effects of room disturbances. The flames were attached at the burner exit by using a small flow of hydrogen, which was introduced through a slot just below the burner exit.

3.2.2 Instrumentation

Measurements were limited to mean concentrations of major gas species and laser extinction by soot to find soot volume fractions. Methods will be only briefly described since they were similar to past work (Gore and Faeth, 1987a,b).

Sampling and analysis with a gas chromatograph were used to measure mean concentrations of major gas species. A water-cooled probe, having an inlet diameter of 6.3 mm, was used for sampling. Sampling rates were crudely isokinetic, based on measured mean velocities along the axis and predictions of radial variations of velocity. This was adequate, however, since effects of doubling and halving sampling rates were small in comparison to experimental uncertainties. The construction of the probe and the sampling system, and the column arrangement and calibration of the gas chromatograph, are described by Gore (1986). Uncertainties in composition measurements (95 percent confidence) are less than 15 percent for concentrations greater than 0.1 percent (by volume), rising to 50 percent at concentrations of 0.01 percent and becoming inversely proportional to concentration at lower concentrations. These uncertainties are largely governed by uncertainties in measuring gas chromatograph peak areas (Gore, 1986). Mixture fractions were computed from these measurements, based on the measured concentrations of carbon and nitrogen and assuming that carbon/hydrogen ratios of the original fuel were preserved throughout the flow field. Uncertainties in these estimates (95 percent confidence) range from 100 percent at $f \sim 5 \times 10^{-4}$ to 30 percent at $f \sim 5 \times 10^{-2}$, and are roughly proportional to the mixture fraction in the intervening region. The uncertainties of the mixture fraction determinations are largely due to uncertainties of gas species concentrations and effects of fuel carbon in soot.

Laser extinction was measured using a helium-neon laser (632.8 nm), similar to earlier work (Gore and Faeth, 1987a,b). Two-wavelength measurements showed that soot particles in these flames approximated the small-particle Rayleigh scattering limit (Gore and Faeth, 1987b). A chopper, operated at 800 Hz, was used to control background and flame radiation and to improve signal-to-noise ratios. Uncertainties in mean extinction measurements (95 percent confidence) are estimated to be less than ten percent, largely governed by finite sampling times (Gore, 1986).

Turbulent fluctuations have only a small effect on laser extinction measurements for these flames (Gore and Faeth, 1987a,b). Therefore, the extinction measurements were deconvoluted to provide estimates of mean soot volume fractions, using the approach described by Santoro et al. (1983a,b). In order to be consistent with earlier work (Gore and Faeth, 1987a,b; Santoro et al. 1983a,b) soot volume fractions were computed using the soot refractive index measurements of Dalzell and Sarofim (1969), i.e., m = 1.547 - 0.56 i at 632.8 nm. Uncertainties in soot volume fraction measurements depend on the fuel and position in the flames. They were estimated by perturbing the deconvolution calculations by the uncertainties of the extinction measurements. The uncertainties (95 percent confidence) can be expressed in terms of the soot volume fractions for each fuel, as follows: acetylene, 15 percent at 4 ppm and 300 percent at 0.06 ppm; ethylene, 20 percent at 0.5 ppm and 300 percent at 0.004 ppm. Uncertainties are roughly proportional to soot volume fractions in the intervening region. Potential errors in estimations of refractive indices, and effects of Mie scattering introduce additional uncertainties, which will be discussed later.

3.2.3 Test Conditions

Table 4 is a summary of the test conditions. Two flames, each, were considered for ethylene and acetylene. The test conditions were identical to Gore and Faeth (1987a,b); therefore, it was not necessary to repeat measurements of initial conditions and the velocity field, which are needed to initiate calculations and to verify flow predictions.

All flows had relatively high initial Reynolds numbers and were turbulent at the burner exit. Initial Richardson numbers were relatively low; however, effects of buoyancy were important for much of the flow, since the surroundings were still. Thus, the radiative heat loss fractions of the flames are relatively independent of burner flow rate, which is characteristic of buoyant turbulent diffusion flames (de Ris, 1978).

The present flames are similar to the longer residence time flames considered by Becker and Liang (1983). They identify their measurements by Richardson ratios and characteristic residence times based on visible flame lengths. The present flames roughly correspond to Richardson ratios on the order of 10^3, or characteristic residence times of 90-160s (based on the definitions of these parameters of Becker and Liang (1983)). Thus, the present flames are in the plateau region observed by Becker and Liang (1983), where radiative heat loss fractions and soot generation efficiencies are nearly independent of the burner flow rate.

Table 4. Test Conditions for Luminous Diffusion Flames[a]

Fuel	Ethylene		Acetylene	
Reynolds number[b]	6,370	12,740	5,300	9,200
Richardson number[c] × 10^4	1.8	0.38	4.5	1.4
$\bar{u}_o$ (m/s) estimated[d]	17.0	33.9	10.5	18.1
$\bar{u}_o$ (m/s) measured	16.7	36.1	11.8	20.6
$k_o^{1/2} / u_o$	0.050	0.048	0.13	0.13
Heat release rate (kW)	13.5	27.0	10.5	18.1
Radiative heat loss fraction (%)	36.0	34.4	57.0	59.0
Fuel flow rate (mg/s)	310	620	217	376
Hydrogen flow rate (mg/s)	1.9	9.6	1.9	1.9

[a] Flow directed vertically upward from a 5-mm diameter passage in still air at normal temperature and pressure. Commercial grade ethylene (Linde Division of Union Carbide) and acetylene (Detroit Welding Supply).

[b] $Re = \bar{u}_o d / \upsilon$ based on fuel-gas properties at burner exit.

[c] $Ri = ad / \bar{u}_o^2$.

[d] $u_o = 4 \dot{m}_o / (\pi d^2 \rho)$ based on fuel-gas density at burner exit.

3.3 Theoretical Methods

Analysis of flame structure was similar to the analysis of nonluminous flames and will be only briefly described. Major assumptions of the structure analysis are as follows: low Mach number boundary-layer flow with no swirl; equal exchange coefficients of all species and heat; buoyancy only affects the mean flow; negligible changes of potential energy; and radiant heat loss from each element of the flow taken to be the same fraction of the chemical energy transformation of the element as the flame as a whole. All these assumptions are either justified by the present test conditions or by acceptable performance in the past. The most questionable assumption involves ignoring radiant energy exchange within the acetylene flames. These flames lose a large fraction, ca. 60 percent, of their energy release of reaction by radiation, suggesting significant coupling between structure and radiation properties. Nevertheless, the approximation was still adopted, in order to avoid the complications of combined structure and radiation analysis for the present.

Flow properties were found using a Favre-averaged k-ε-g turbulence model proposed by Bilger (1976), with specific modifications and empirical constants due to Jeng and Faeth (1984a). The laminar flamelet approximation for diffusion flames was used to relate scalar properties to the mixture fraction, following Bilger (1977). State relationships for the concentrations of major gas species, soot volume fractions, temperature, and density were obtained from the earlier studies (Gore and Faeth, 1987a,b).

Initial conditions for the structure calculations were developed by linear extrapolation of measurements of mean and fluctuating velocities at x/d = 2 (Gore and Faeth, 1987b). Similarly, the specification of boundary conditions, and the details of the numerical computations, follow past practice.

3.4 Results and Discussion

3.4.1 Acetylene/Air Flames

Properties along axis. Measurements and predictions of mean and fluctuating velocities, and mean concentrations of major gas species, along the axis of the turbulent acetylene/air diffusion flames, are plotted as a function of distance in Figs. 14 and 15. Interference from strong flame luminosity and absorption of scattered and incident laser light by the soot particles posed some difficulties for the LDA measurements. Photomultiplier cathode voltage had to be set at a low value, ca. 200 V, and large amplification of the filtered signal on the preprocessor had to be used to obtain valid samples. The measurements in the heavily sooty regions (ca. x/d = 30 to x/d = 60), are somewhat biased towards higher mean velocities and lower fluctuating velocities due to the unavoidable Doppler signals from the soot particles. The LDA measures time-averaged velocities while the analysis predicts

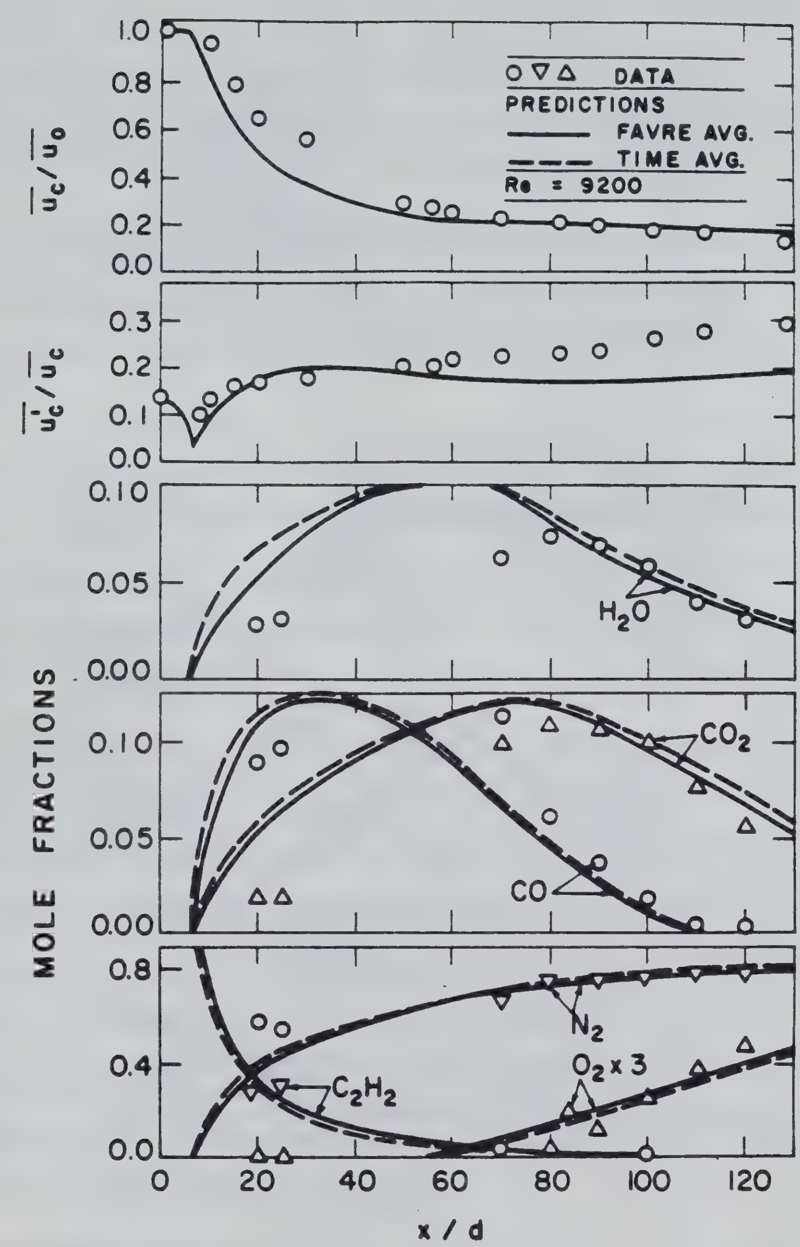

Figure 14. Properties along axis of acetylene/air diffusion flame (Re = 9,200).

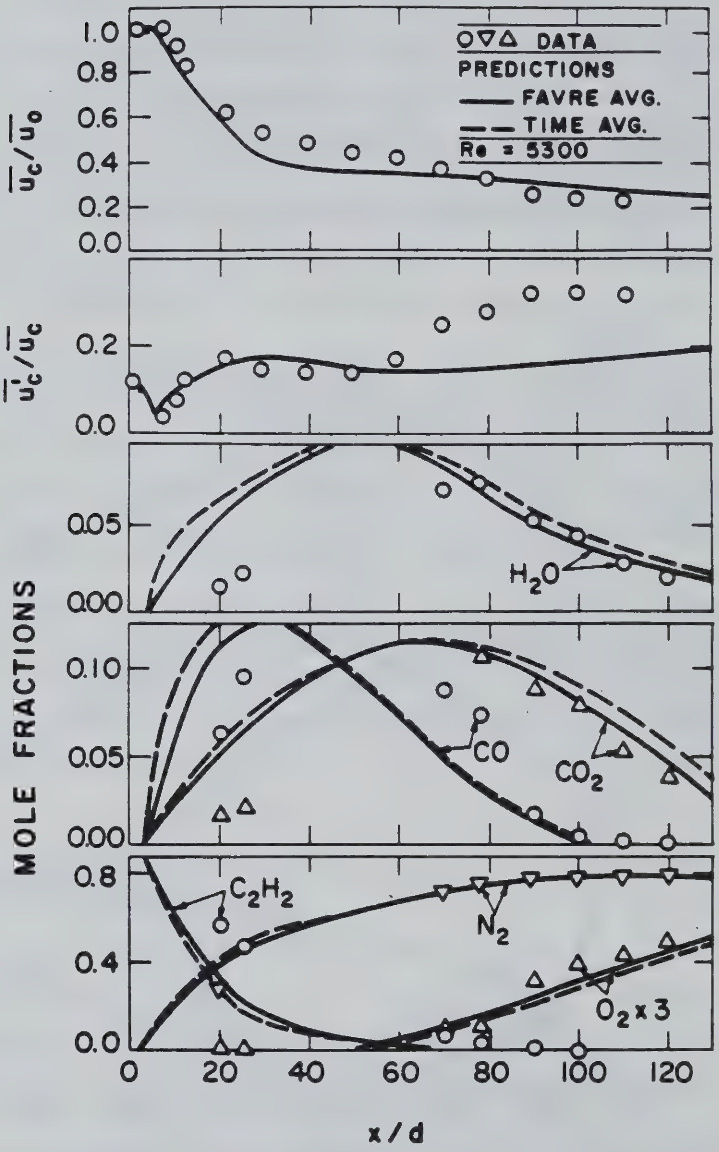

Figure 15. Properties along axis of acetylene/air diffusion flame (Re = 5,300).

Favre-averaged quantities, and effects of buoyancy/turbulence were ignored during present predictions, as noted earlier. In view of these difficulties, the agreement between measurements and predictions is reasonable.

Gas samples for species concentration measurements were obtained using the 6.3 mm diameter (large) sampling probe. Samples could not be obtained in the very sooty areas; this accounts for gaps in the data. Both Favre- and time-averaged predictions are shown, but they do not differ very much. The comparison between predictions and measurements is generally similar to results for nonluminous flames discussed earlier.

Species concentrations. Differences between time- and Favre-averaged predictions of scalar properties are less than 15 percent for present test conditions. Such differences are comparable to experimental uncertainties; therefore, only Favre-averaged predictions of mixture fractions and species concentrations are illustrated in the following, in order to reduce cluttering of the figures.

Figure 16 is an illustration of predicted and measured mean mixture fractions for the two turbulent acetylene/air flames. Results are plotted as a function of r/x (the similarity variable most frequently used for turbulent jets and plumes) at various heights above the burner exit. The flame tips (based here and in the following on the location of the mean stoichiometric mixture ratio along the axis) are reached at x/d ~ 75 and 80 for the low and high Reynolds number flames (see Figs. 14 and 15).

The coordinates used in Fig. 16 provide a direct indication of flow widths and levels of mixing in the flames; therefore, plots of this type are sensitive indicators of the performance of turbulent mixing analysis. The agreement between predictions and measurements, and predicted trends with respect to burner Reynolds numbers, are both reasonably good. The largest discrepancies between predictions and measurements are at x/d = 130 for the lower Reynolds number flame, where measured mixture fractions are well below predictions. This behavior is probably due to ambient disturbances which deflect the flow, reducing apparent concentration levels of fuel-containing species; this effect is particularly difficult to control in weak flows far from the burner. In general, the performance of the analysis is consistent with earlier findings along the axis of these flames, and is characteristic of earlier evaluations of similar predictions for a variety of other turbulent diffusion flames (Gore et al., 1987a,b,c; Jeng and Faeth, 1984a,b; Jeng et al., 1982, 1984).

Typical predictions and measurements of the concentrations of major gas species (N_2, O_2, C_2H_2, CO, CO_2) are illustrated in Figs. 17-20. Mean species mole fractions are plotted as a function of r/x for x/d = 53, 80, 110 and 130. The results suggest no particular difficulty with the laminar flamelet concept for gas species in these heavily sooting flames. The comparison between predictions and measurements is similar to non-hydrocarbon flames

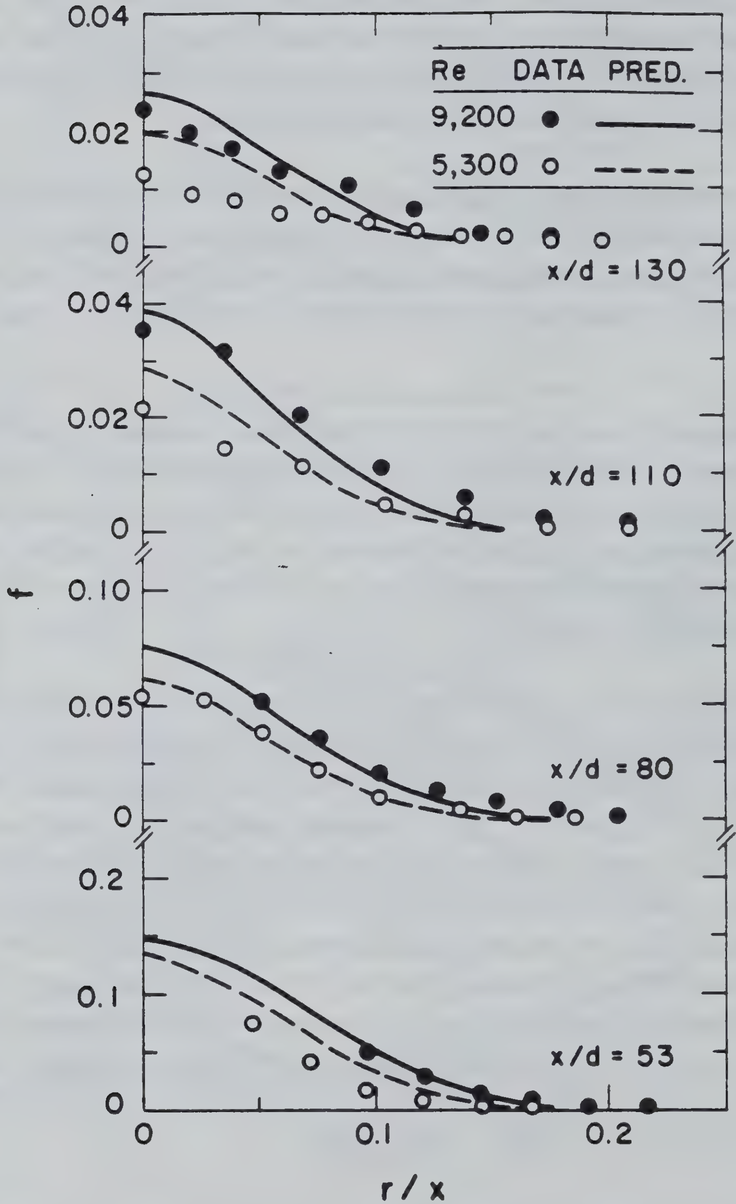

Figure 16. Mean mixture fraction distributions in acetylene/air diffusion flames.

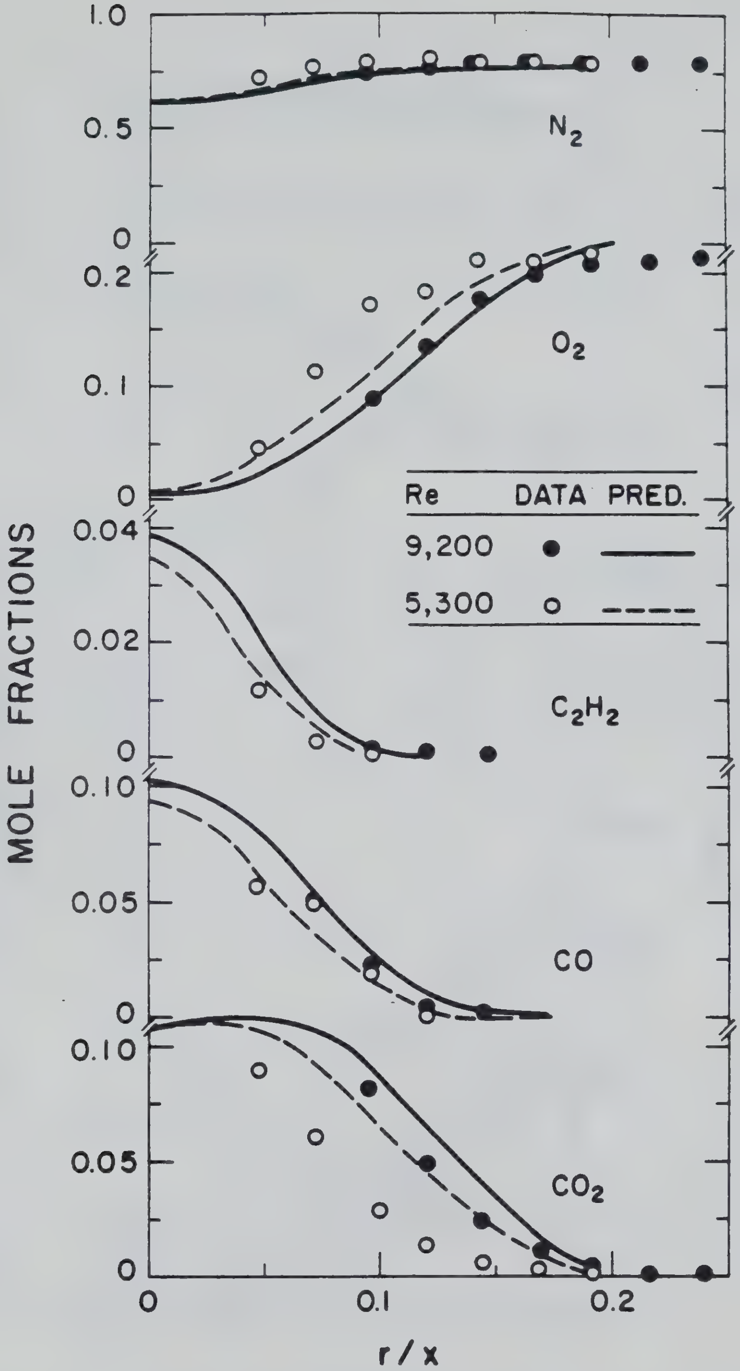

Figure 17. Mean gas species concentrations in acetylene/ air diffusion flames (x/d = 53).

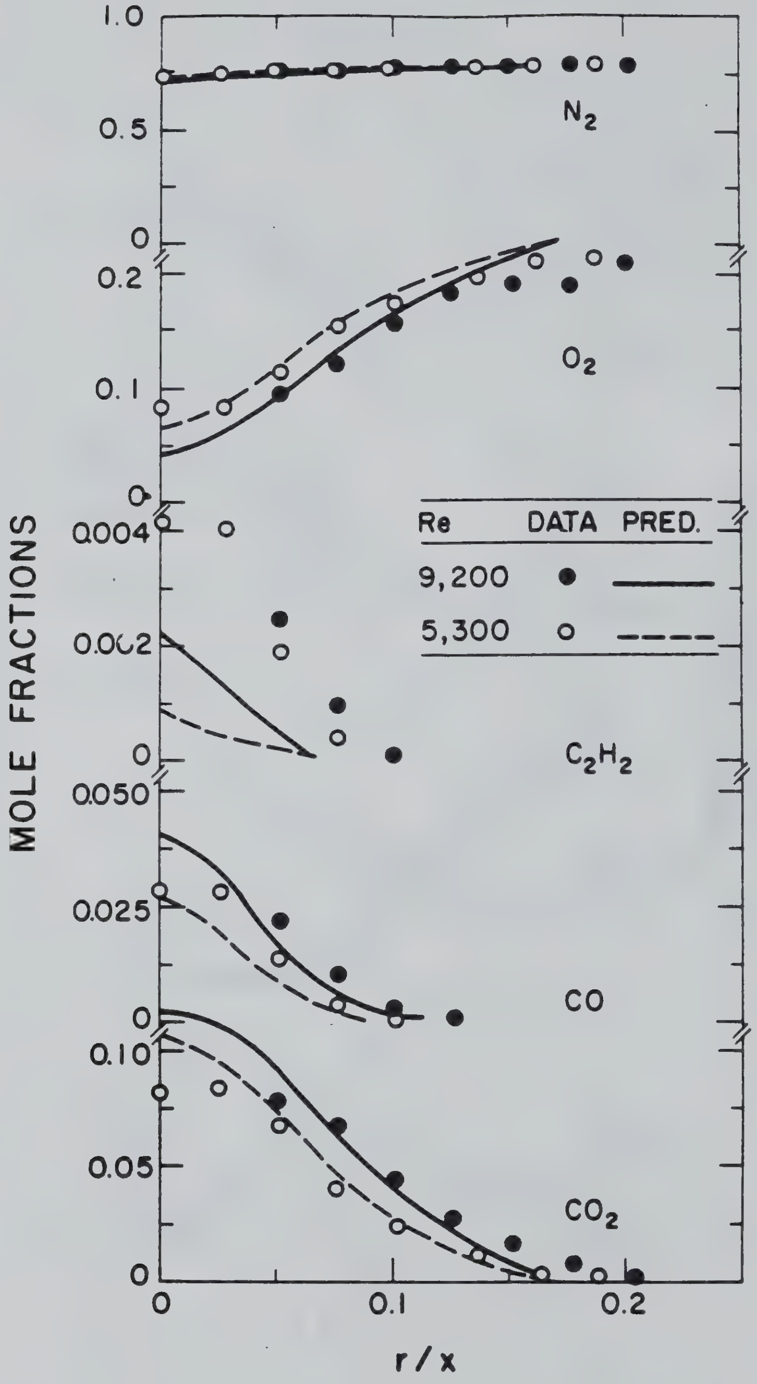

Figure 18. Mean gas species concentrations in acetylene/ air diffusion flames (x/d = 80).

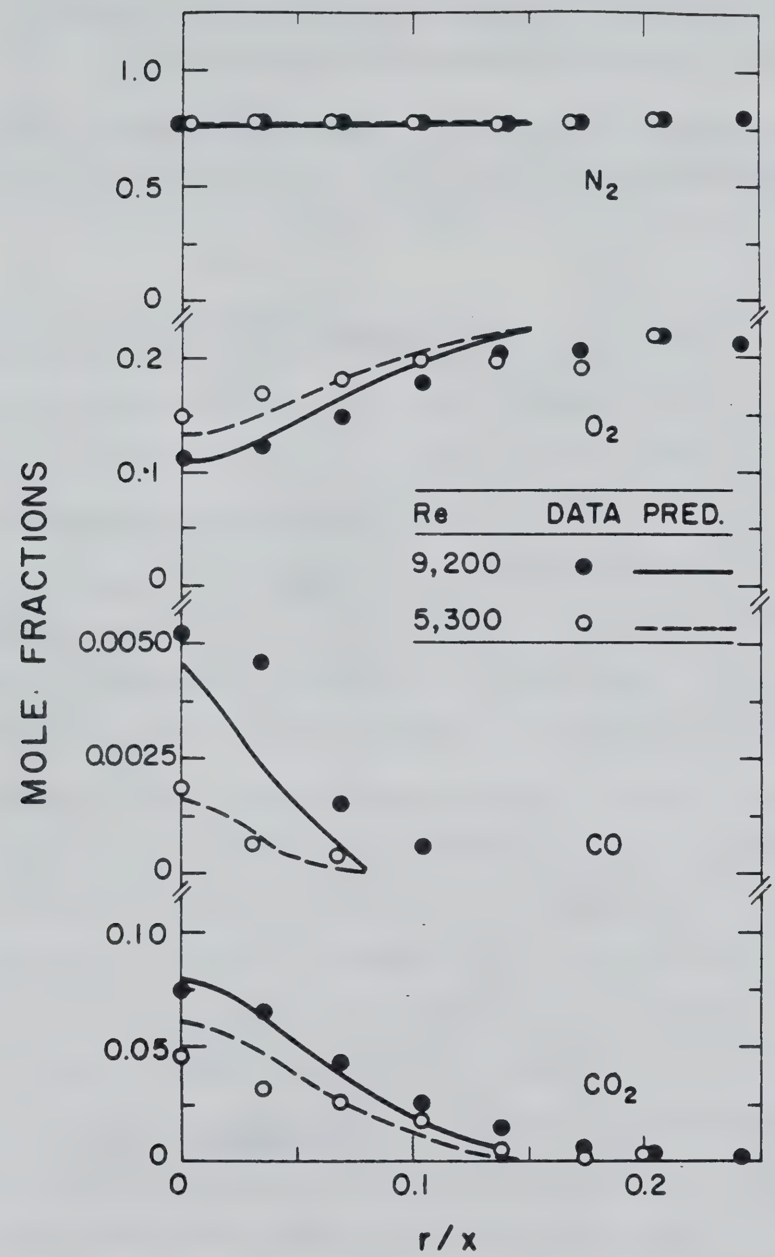

Figure 19. Mean gas species concentrations in acetylene/air diffusion flames (x/d = 110).

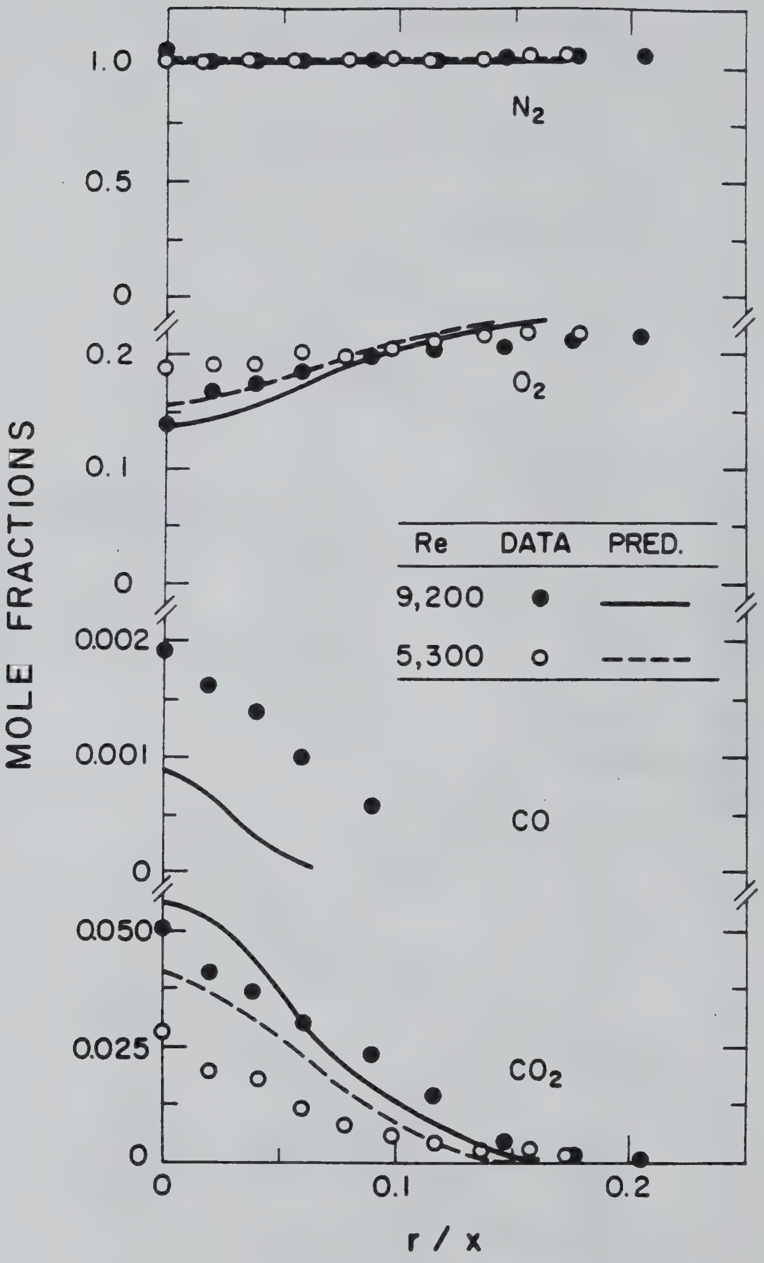

Figure 20. Mean gas species concentrations in acetylene/ air diffusion flames (x/d = 130).

where local thermodynamic equilibrium is essentially maintained (Gore et al., 1987b,c). Areas of discrepancies between predictions and measurements generally are associated with regions where errors are present in the mixture fraction predictions illustrated in Fig. 16. It should be noted, however, that present measurements emphasize the overfire (lean) region of the flames, where local thermodynamic equilibrium is also a reasonably good approximation, based on measurements in laminar acetylene/air diffusion flames (Gore and Faeth, 1987b).

Soot volume fraction distributions. Time-averaged predictions of soot volume fractions are reported in the following, in order to be consistent with the measurements. Predictions are based on the soot volume fraction state relationships of Gore and Faeth (1987b).

Predicted and measured time-averaged soot volume fractions in the turbulent acetylene flames are plotted in Fig. 21 as a function of r/x, for various heights above the burner exit. Trends with respect to position and Reynolds number are predicted reasonably well in both the flaming and overfire regions of the flow, using the single soot volume fraction state relationship. Differences between predictions and measurements are generally comparable to experimental uncertainties and they are certainly comparable to the anticipated performance of the predictions in view of the approximation of turbulence model used to predict flame structure. The greatest differences between predictions and measurements are observed at x/d = 53, where predictions overestimate the width of the soot-containing region. Difficulties with the mixing analysis are probably the main cause of this problem, e.g., profile widths of all other scalar properties are somewhat overestimated at this position, see Figs. 16 and 17.

Correlation of soot volume and mixture fractions. Predictions and measurements of soot volume fractions are cross-plotted directly as a function of mixture fraction (the soot volume fraction state relationship coordinates) in Fig. 22. The measurements are identified by flame Reynolds number and height above the source, but not by radial position, in order to reduce cluttering. The measurements represent time-averaged soot volume fractions as a function of mean mixture fractions as measured by the sampling system. As noted earlier, the mixture fraction measurements have indeterminant levels of density weighting but should fall between time and Favre averages, which are not very different for the conditions illustrated in Fig. 22. Experimental uncertainties, estimated as described earlier, are indicated by the crossed brackets located at both ends of the data range. The present measurements are limited to overfire (lean) conditions, due to problems of measuring species concentrations in the flaming region, where soot concentrations are high.

Several correlations and predictions are also plotted in Fig. 22. This includes the lean portion of the soot volume fraction state relationship, found earlier (Gore and Faeth, 1987b), constructed for the limits of an adiabatic flame and a flame losing the measured radiative heat loss fraction. Differences between these limits are most significant near stoichiometric conditions, where the correlation allowing for radiative heat losses is probably most

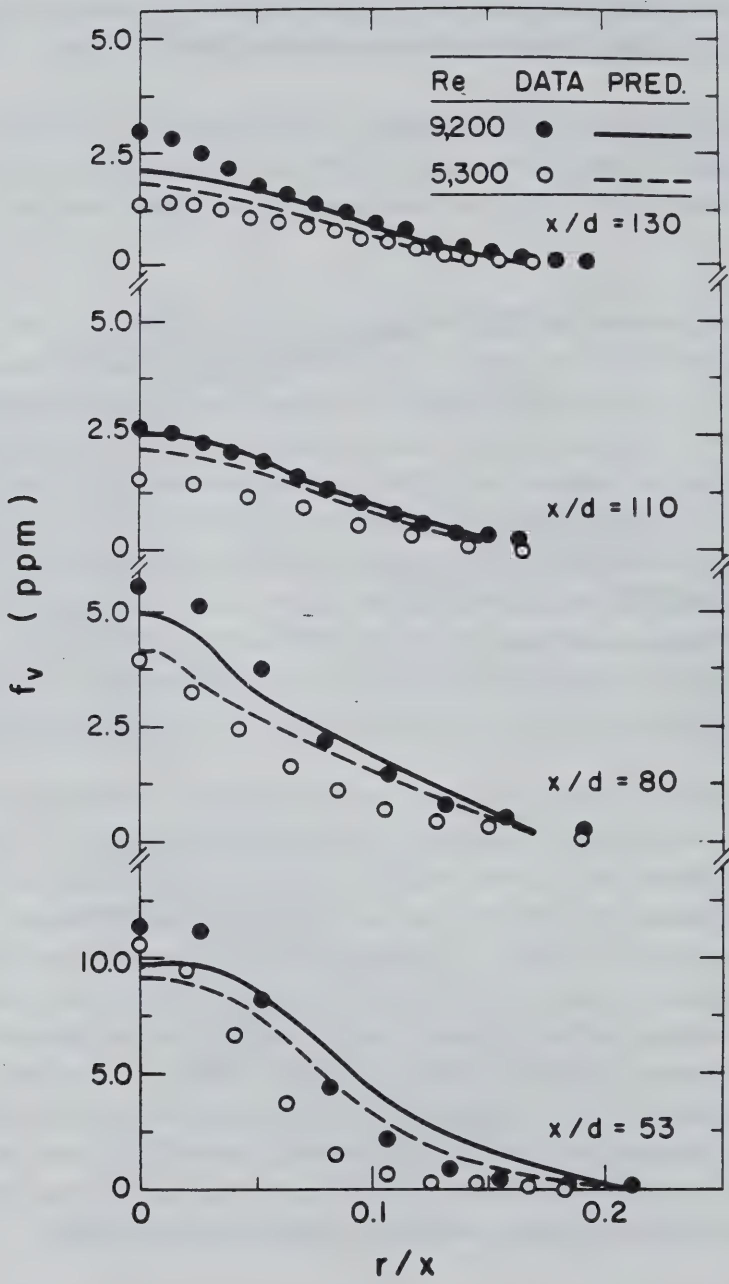

Figure 21. Mean soot volume fraction distributions in acetylene/air diffusion flames.

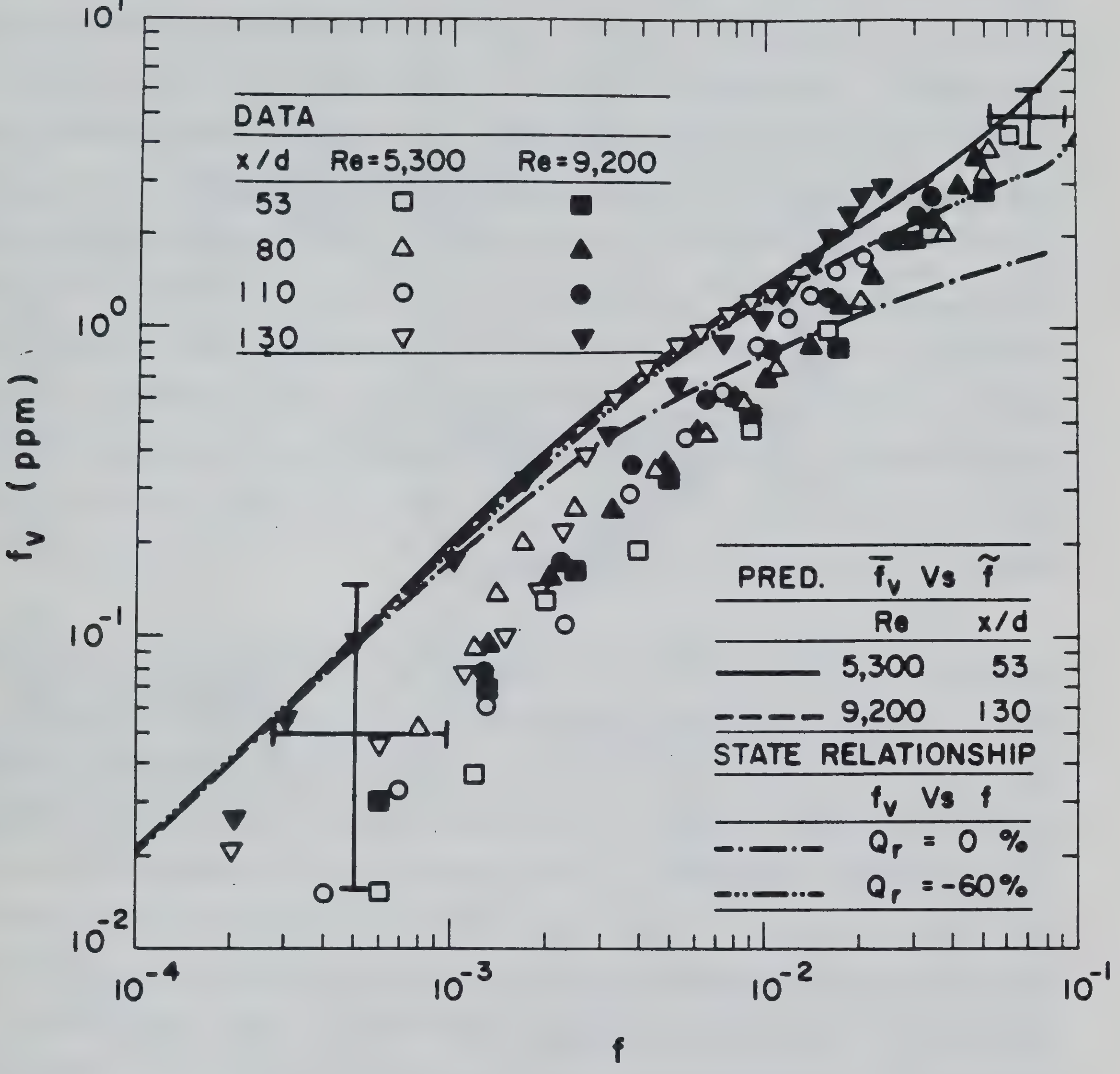

Figure 22 Correlation between soot volume fractions and mixture fractions in the overfire region of acetylene/air diffusion flames (the stoichiometric mixture fraction is 0.0702).

representative.

Relating time-averaged measurements in a turbulent flame to the instantaneous properties associated with a state relationship is questionable; therefore, potential effects of turbulent fluctuations have been illustrated in Fig. 22 by cross-plotting predictions of time-averaged soot volume fractions and Favre-averaged mixture fractions in an attempt to simulate the measurements. These predictions were based on the standard soot volume fraction state relationships, allowing for radiative heat losses. For acetylene, changes in burner Reynolds numbers and height above the burner exit had little effect on these plots, e.g., the two predictions illustrated in Fig. 22 bound all the results and are essentially identical. Effects of turbulent fluctuations are small for very lean conditions, where the time-averaged predictions for the turbulent flames merge with the state relationships. As stoichiometric conditions are approached, however, the turbulent predictions are biased above the soot volume fraction state relationship, due to the presence of the soot spike on the fuel-rich side of the stoichiometric mixture fraction. The soot spike is illustrated in Fig. 23, where measurements in laminar flames from Gore and Faeth (1987b) are used to develop the soot volume state relationship for fuel-rich conditions. The correlation for fuel-rich conditions is seen to be relatively crude with departure from universality at near burner conditions. Nevertheless, soot in the fuel-rich region is clearly confined to a relatively narrow-range of mixture fractions with relatively constant maximum values of soot volume fractions.

The soot volume and mixture fraction measurements illustrated in Figs. 22 and 23 appear to be correlated along single lines at each burner flow rate and height above the burner. This behavior, however, is an artifact of the measurements, since all the soot volume fractions at a given flow rate and position are related to some extent through the deconvolution procedure. Otherwise, measurements at various burner flow rates and heights above the burner appear to be randomly distributed, with soot volume fractions and mixture fractions being correlated within experimental uncertainties. Present measurements are consistently below the state relationship of Gore and Faeth (1987b) at low mixture fractions, where effects of heat losses and turbulent fluctuations are small. However, the differences are within experimental uncertainties so that advocating an alternative correlation is questionable, particularly since the correlation of Gore and Faeth (1987b) performed reasonably well for predictions of soot volume fraction distributions illustrated in Fig. 21. As mixture fractions approach stoichiometric conditions, the present measurements trend above the state relationships, roughly following the predictions of effects of turbulent fluctuations in this region. Overall, the findings are supportive of the existence of nearly universal soot volume fraction state relationships, along the lines proposed by Gore and Faeth (1987b), for the overfire regions of the present turbulent acetylene/air flames.

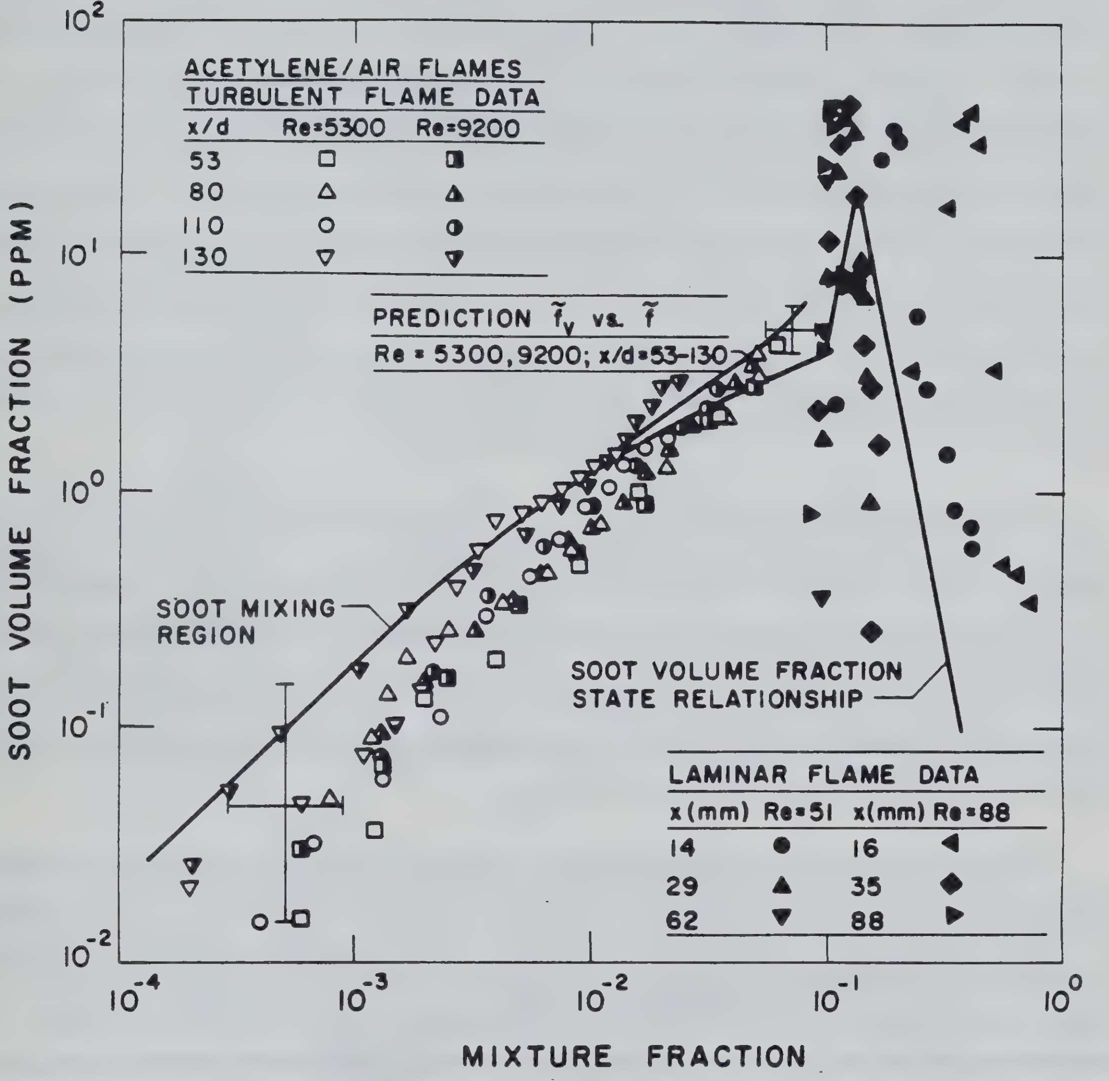

Figure 23. Soot volume fraction state relationship for acetylene/air diffusion flames (the stoichiometric mixture fraction is 0.0702).

3.4.2 Ethylene/Air Flames

Properties along axis. Measurements and predictions of mean and fluctuating velocities, and mean concentrations of major gaseous species along the axis of the two ethylene flames are shown in Figs. 24 and 25. The LDA measurements rely on the scattered signal from the seeding particles but the scattered signal from the soot particles could not be avoided in the highly sooty regions and has probably introduced a bias towards higher mean velocities and lower fluctuating velocities in these regions. However, the measurements and predictions for mean velocities agree reasonably well for both the flames. The measured velocity fluctuations show a reduction, in the case of the higher Reynolds-number flame, probably due to the bias introduced by soot particles. The effects of buoyancy on turbulence in the lower Reynolds-number flame lead to an increase in the velocity fluctuations. The differences between time-averaged measurements and Favre-averaged predictions also account for some of the discrepancies. Measurements of mole fractions of the major gas species, using a large probe in the sooty regions and a small probe in the relatively soot-free areas, are also shown in Figs. 24 and 25. The data from the two probes are in reasonable agreement for points where both probes could be used. Both Favre- and time-averaged predictions are shown; however, the two are not much different and are in reasonable agreement with the data.

Species concentrations. Predicted and measured mean mixture fractions are plotted in Fig. 26 as a function of r/x, for various heights above the burner exit. Flame tips are reached at x/d ~ 85 and 90 for the low and high Reynolds number flames (see Figs. 24 and 25). The comparison between predictions and measurements is not as good as the results for acetylene illustrated in Fig. 16, particularly for the higher Reynolds number ethylene flame where predictions underestimate measured mixture fractions everywhere. The largest discrepancies between predictions and measurements are observed at the highest position, where room disturbances are probably a factor.

Typical predictions and measurements of the mole fractions of major gas species are plotted in Figs. 27-31 as a function of r/x, for x/d = 50, 70, 90, 130 and 150. The comparison between predictions and measurements is similar to the findings for acetylene, with somewhat increased deficiencies being attributable to the poorer predictions of mixing for ethylene, e.g., poorer predictions of mixture fraction distributions in the flames. In view of the approximations of the turbulent mixing analysis, and experimental uncertainties, the state relationships for gas species of Gore and Faeth (1987a) appear to be acceptable for the overfire region of the present turbulent ethylene/air flames.

Soot volume fraction distributions. Time-averaged predictions and measurements of mean soot volume fractions are illustrated in Fig. 32 as a function of r/x, for various heights above the burner exit. Trends with respect to position and Reynolds number are represented reasonably well by a single soot volume fraction state relationship. However, quantitative agreement between predictions and measurements is poorer than for the

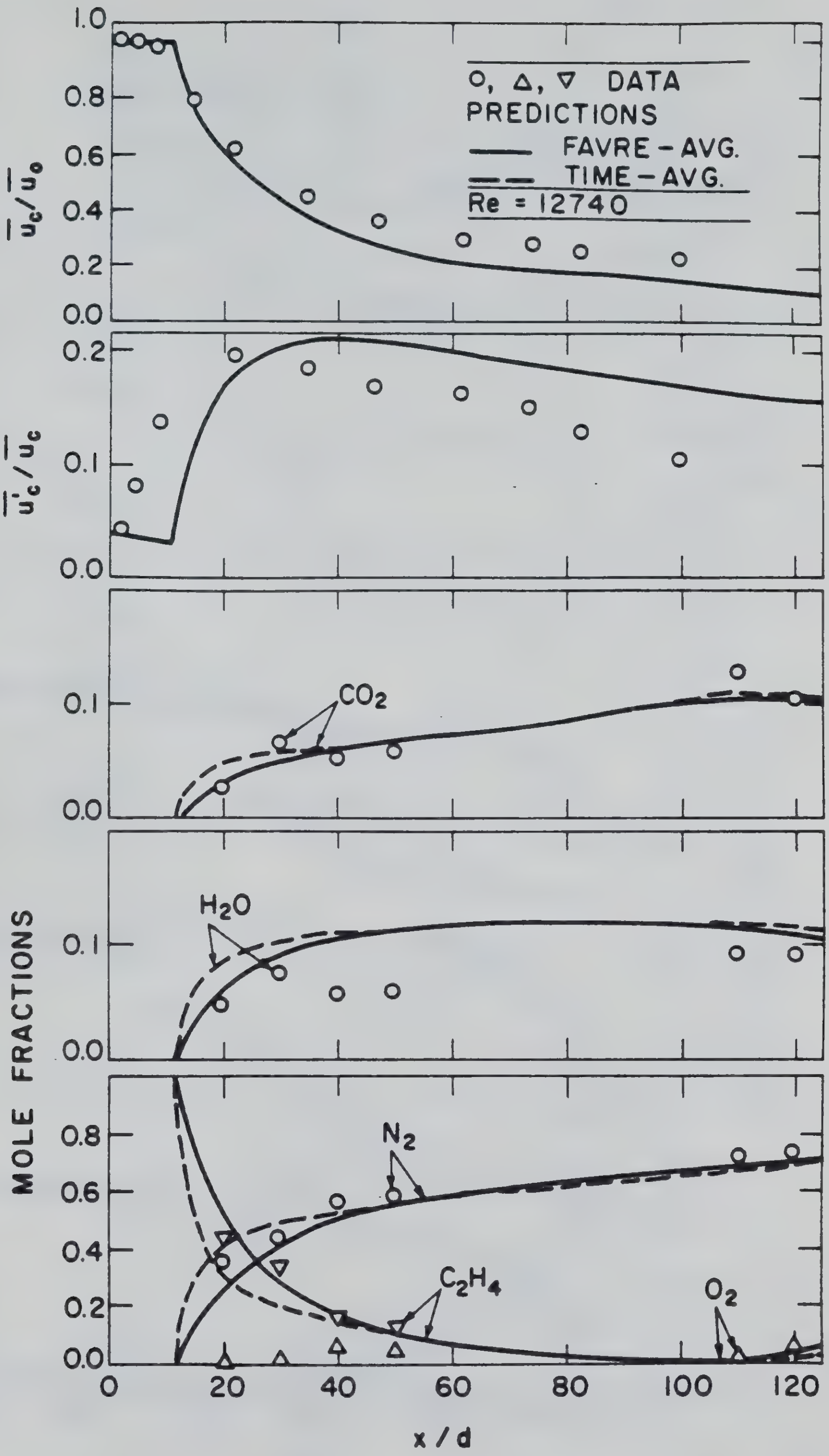

Figure 24. Properties along axis of ethylene/air diffusion flame (Re = 12,740).

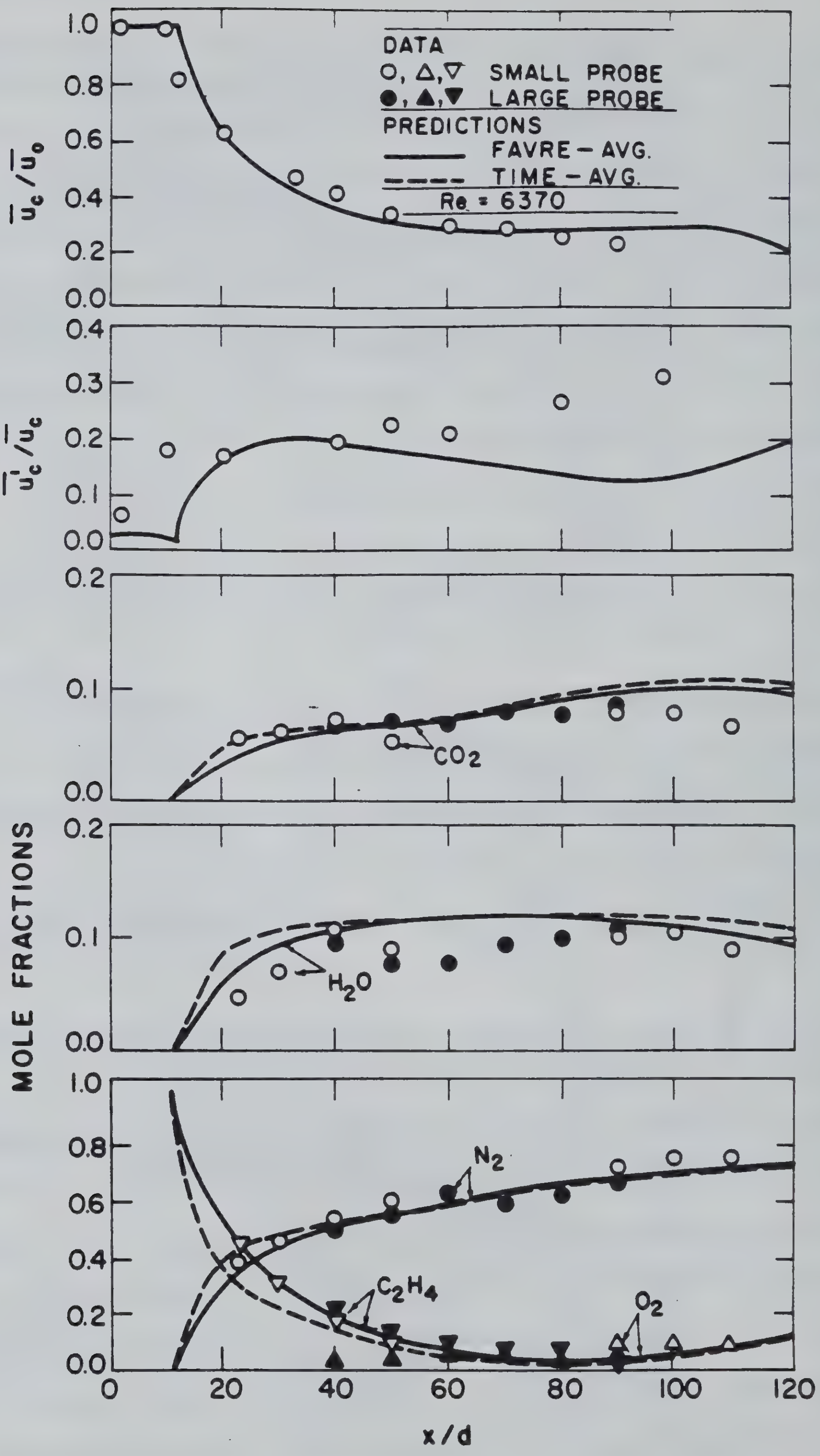

Figure 25. Properties along axis of ethylene/air diffusion flame (Re = 6,370).

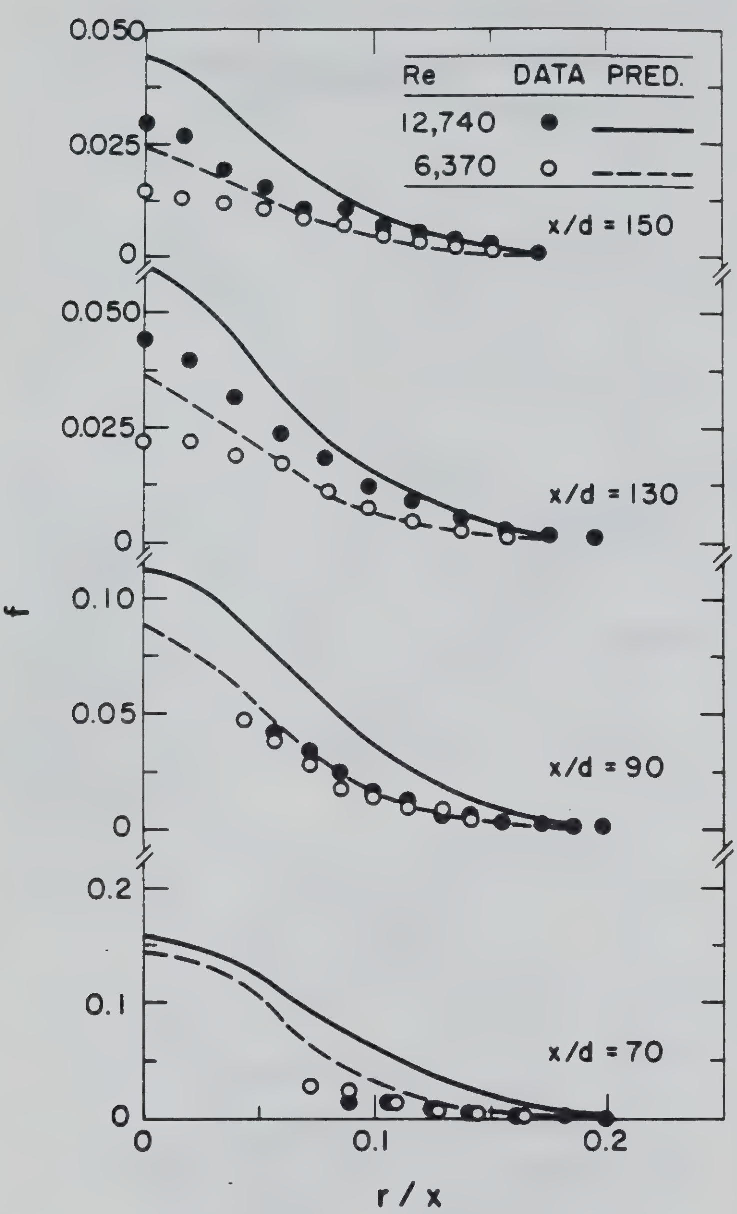

Figure 26. Mean mixture fraction distributions in ethylene/air diffusion flames.

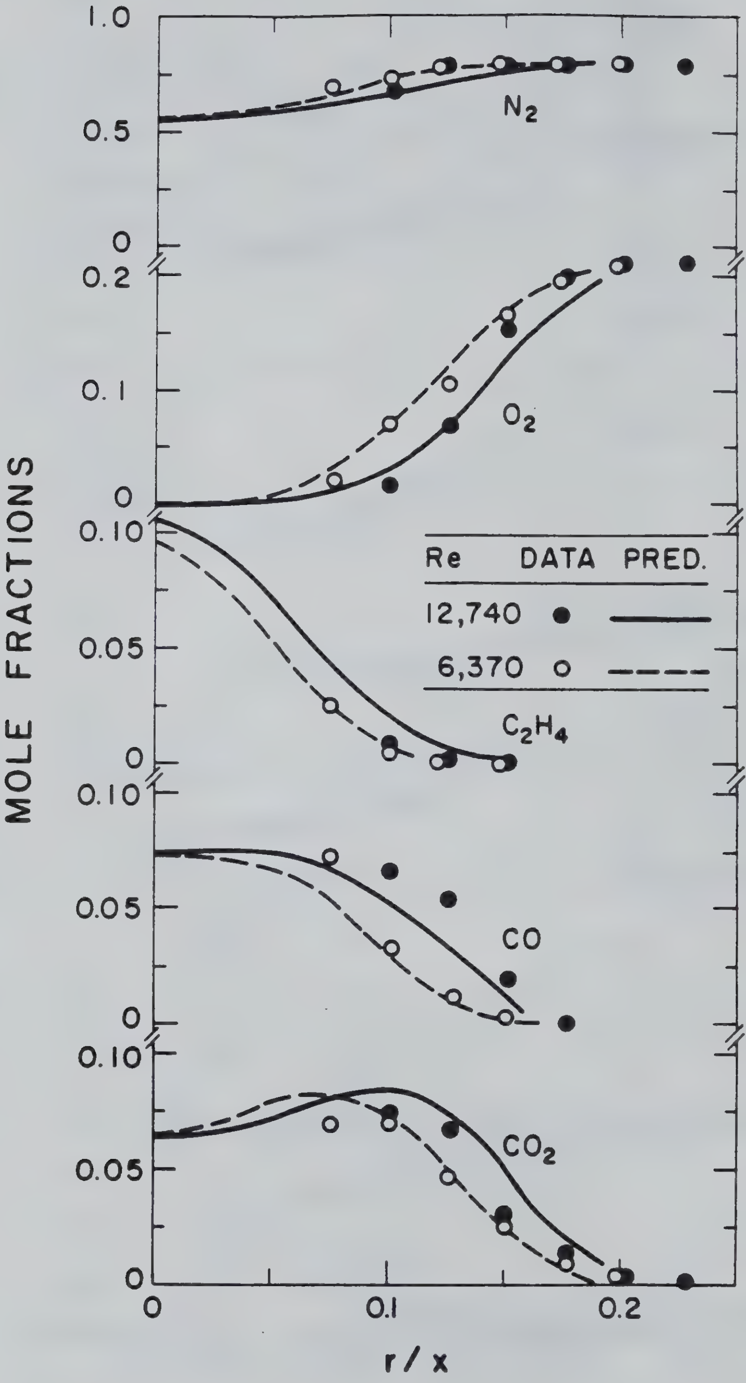

Figure 27. Mean gas species concentrations in ethylene/ air diffusion flames (x/d = 50).

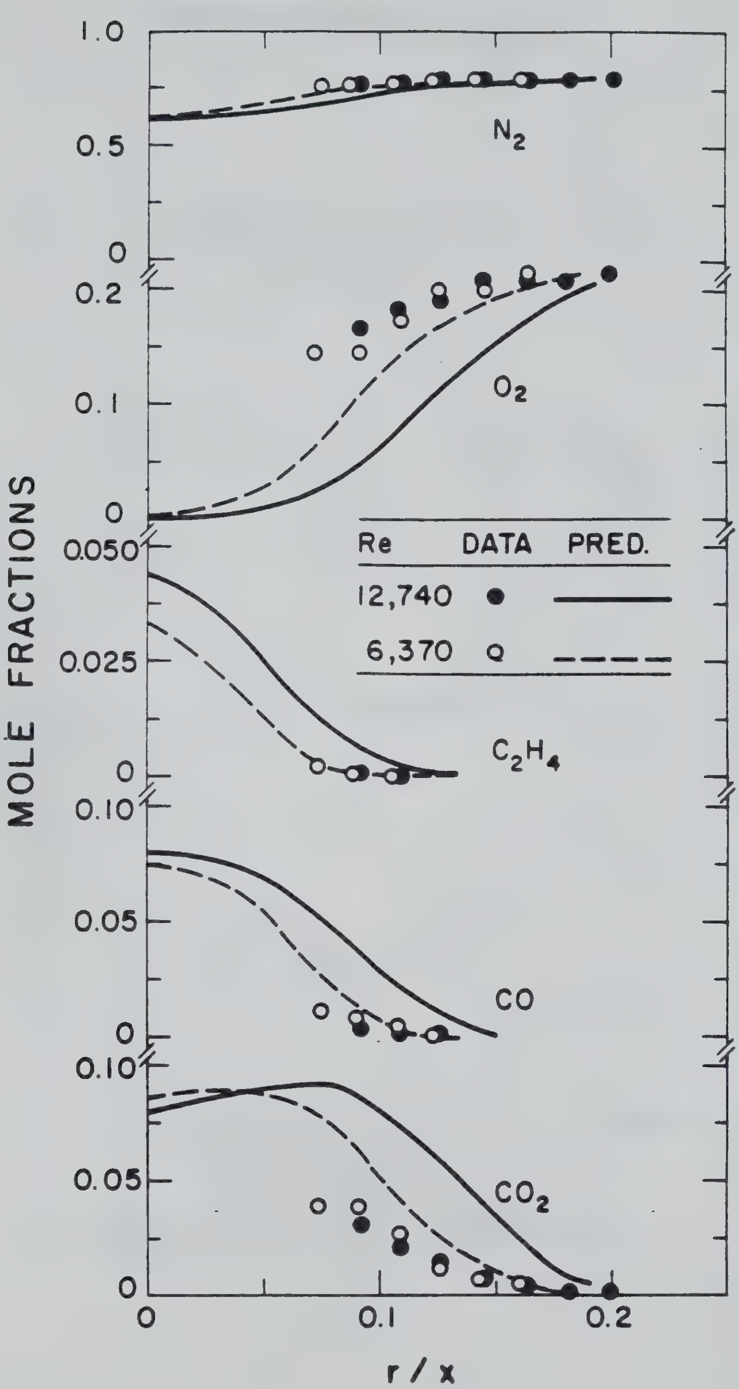

Figure 28. Mean gas species concentrations in ethylene/ air diffusion flames (x/d = 70).

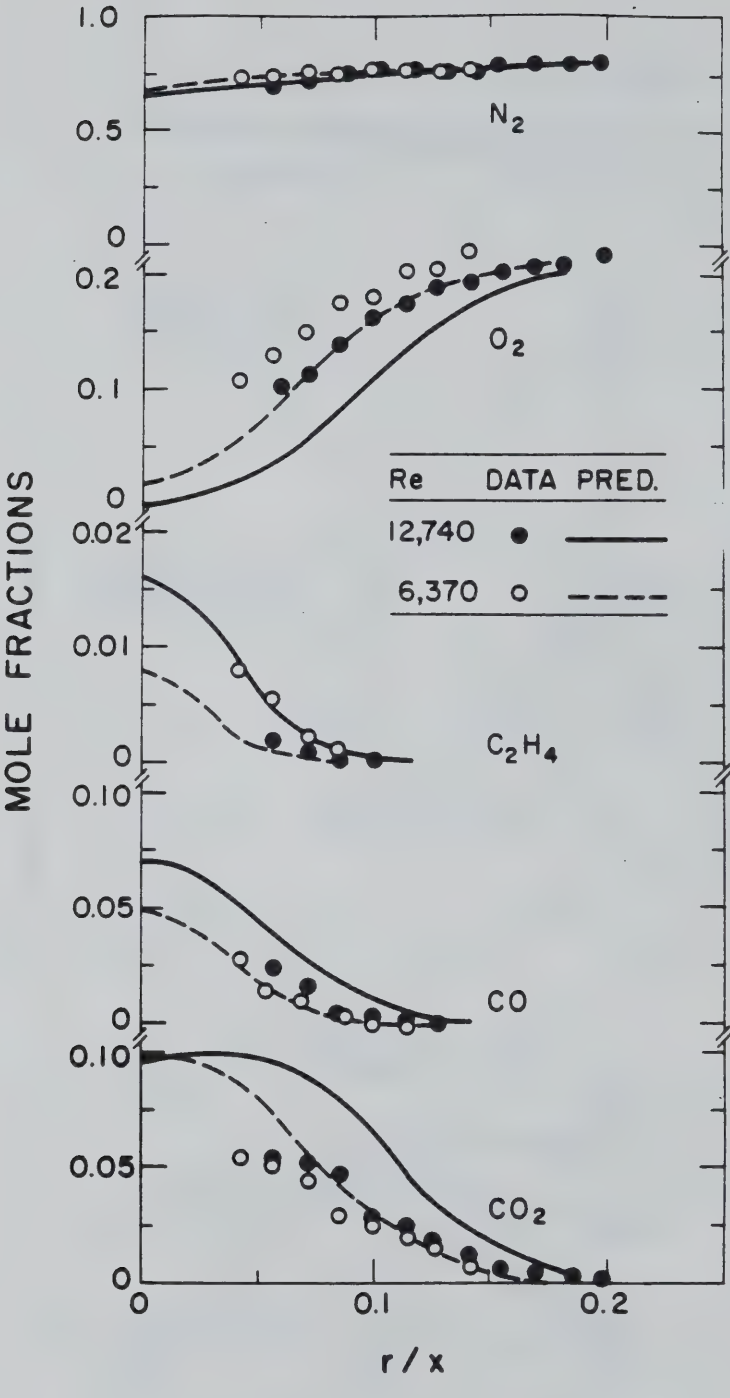

Figure 29. Mean gas species concentrations in ethylene/ air diffusion flames (x/d = 90).

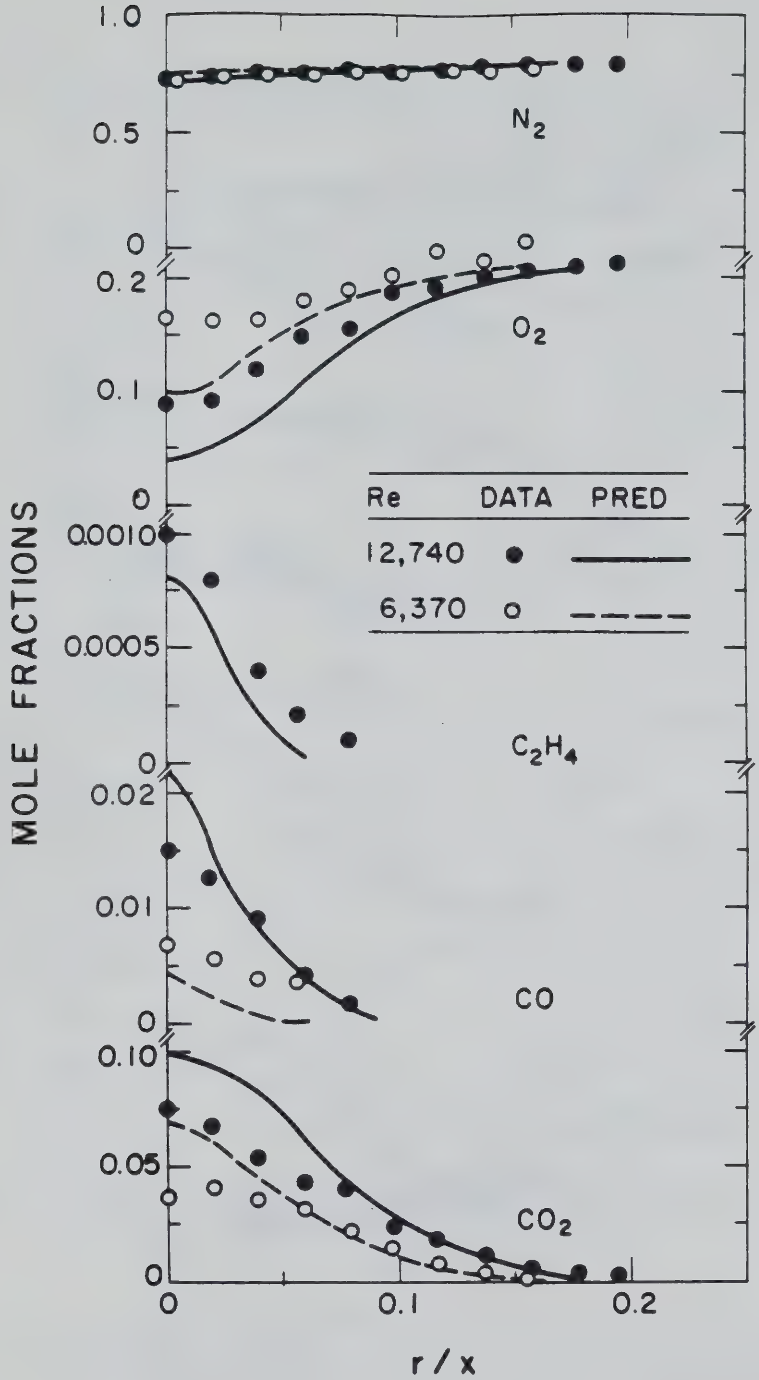

Figure 30. Mean gas species concentrations in ethylene/air diffusion flames (x/d = 130).

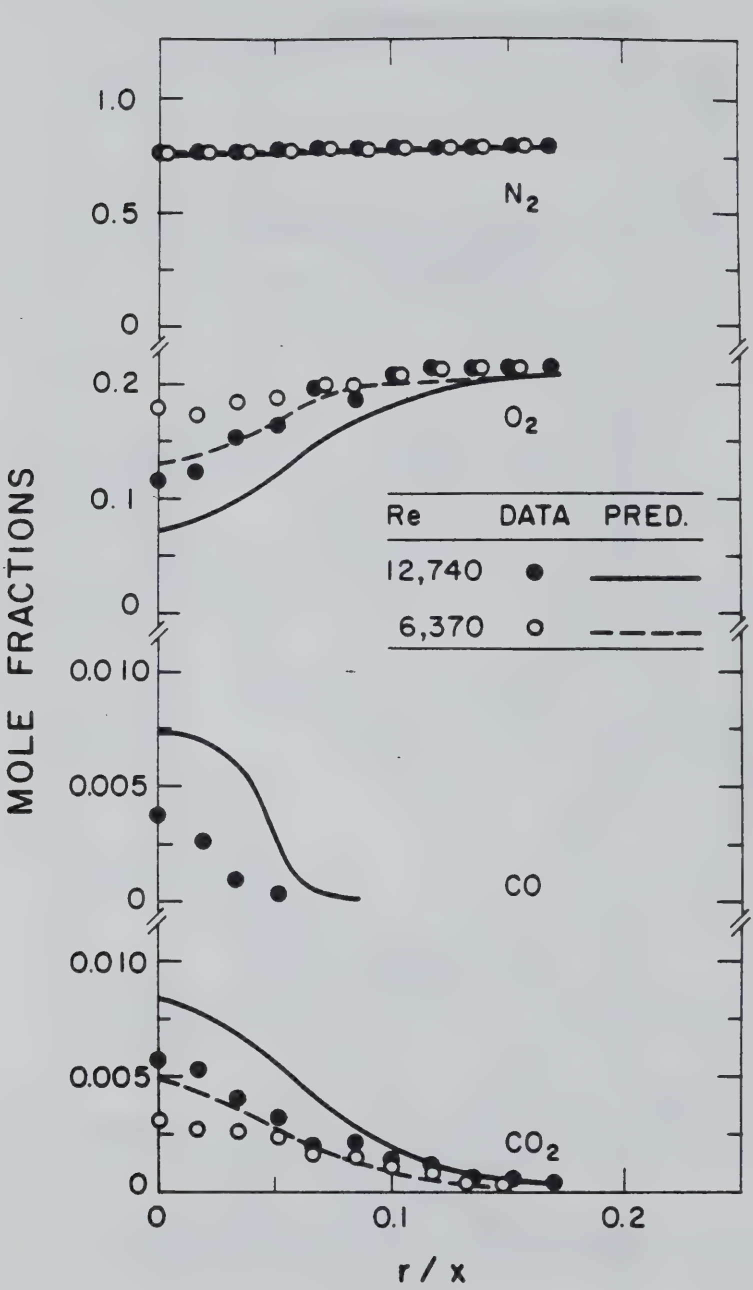

Figure 31. Mean gas species concentrations in ethylene/ air diffusion flames (x/d = 150).

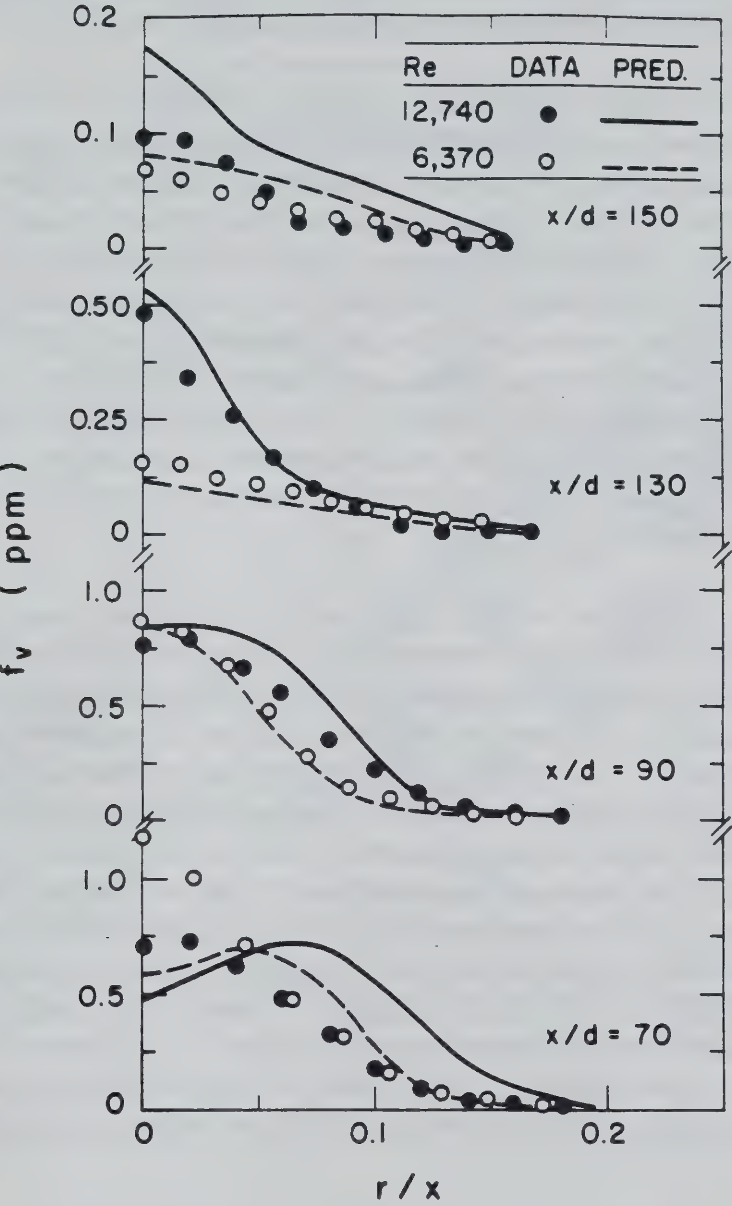

Figure 32. Mean soot volume fraction distributions in ethylene/air diffusion flames.

acetylene/air flames illustrated in Fig. 21. Generally higher experimental uncertainties, since ethylene soot volume fractions are roughly an order-of-magnitude smaller than those of acetylene, is probably a factor in this observation. Room disturbances, coupled with rather large experimental uncertainties, are mainly responsible for the poorer agreement between measurements and predictions at the highest position illustrated in Fig. 32.

Correlation of soot volume and mixture fractions. Measurements and predictions of soot volume fractions and mixture fractions in the overfire region of the ethylene flames are cross-plotted in Fig. 33, similar to the acetylene/air results pictured in Fig. 22. Figure 34 is a similar plot, but adding results for fuel-rich conditions obtained from measurements in laminar flames (Gore and Faeth, 1987a), so that the soot spike can be seen. The predictions near stoichiometric conditions indicate greater biasing of observed time-averaged soot volume fractions above the state relationship, and larger effects of flame Reynolds number and height above the burner on the degree of biasing, due to turbulence, than was observed for acetylene (see Figs. 22 and 23). This behavior is observed since maximum soot concentrations in the soot spike are much higher than soot concentrations in the lean region, and the spike is closer to the stoichiometric mixture fraction, for ethylene than for acetylene (cf. Figs. 23 and 34).

Measurements illustrated in Fig. 33 for the lower Reynolds number flame (open symbols) are similar to the findings for acetylene. The results fall along the soot volume fraction state relationships at low mixture fractions, where effects of turbulent fluctuations and local variations in radiative heat loss fractions are small. As the mixture fraction increases toward the stoichiometric mixture fraction, the measurements are biased upward from the state relationships, similar to the turbulence predictions. Disregarding the apparent correlation of the measurements at each height above the burner, since this is probably caused by their determination from a single deconvolution, these measurements are randomly distributed. For low mixture fractions, the measurements agree with the state relationships well within experimental uncertainties. For high mixture fractions, data scatter is somewhat greater than experimental uncertainties, but this behavior is expected based on the results of the turbulent predictions, due to the effect of height above the burner exit on the degree of biasing of the time-averaged soot volume fractions. Thus, results for the low Reynolds number ethylene flame are generally supportive of a universal soot volume fraction state relationship in the overfire region.

In contrast, results for the high Reynolds number ethylene flame, illustrated in Fig. 33, exhibit much greater scatter. This is particularly true for low mixture fractions, where scatter of the measurements exceeds the rather large range of estimated experimental uncertainties shown on the figure, even though effects of radiative heat losses and turbulent fluctuations are small. This behavior could be an indication of failure of the laminar flamelet concept for soot volume fractions due to effects of finite-rate chemistry. The high Reynolds number flame for ethylene has the shortest characteristic residence time of all the flames considered; while the

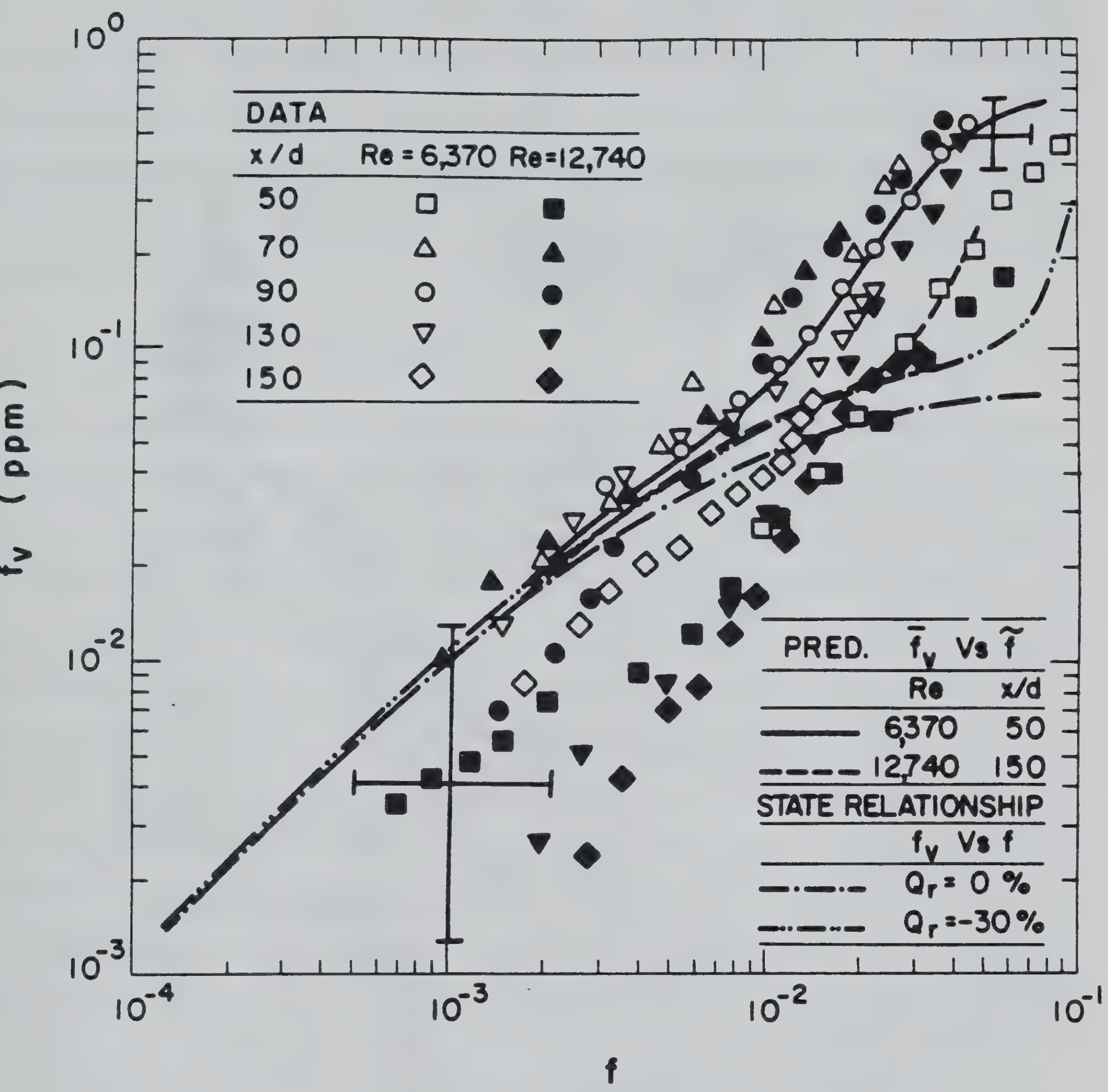

Figure 33. Correlation between soot volume fractions and mixture fractions, in the overfire region of ethylene/air diffusion flames (the stoichiometric mixture fraction is 0.0634).

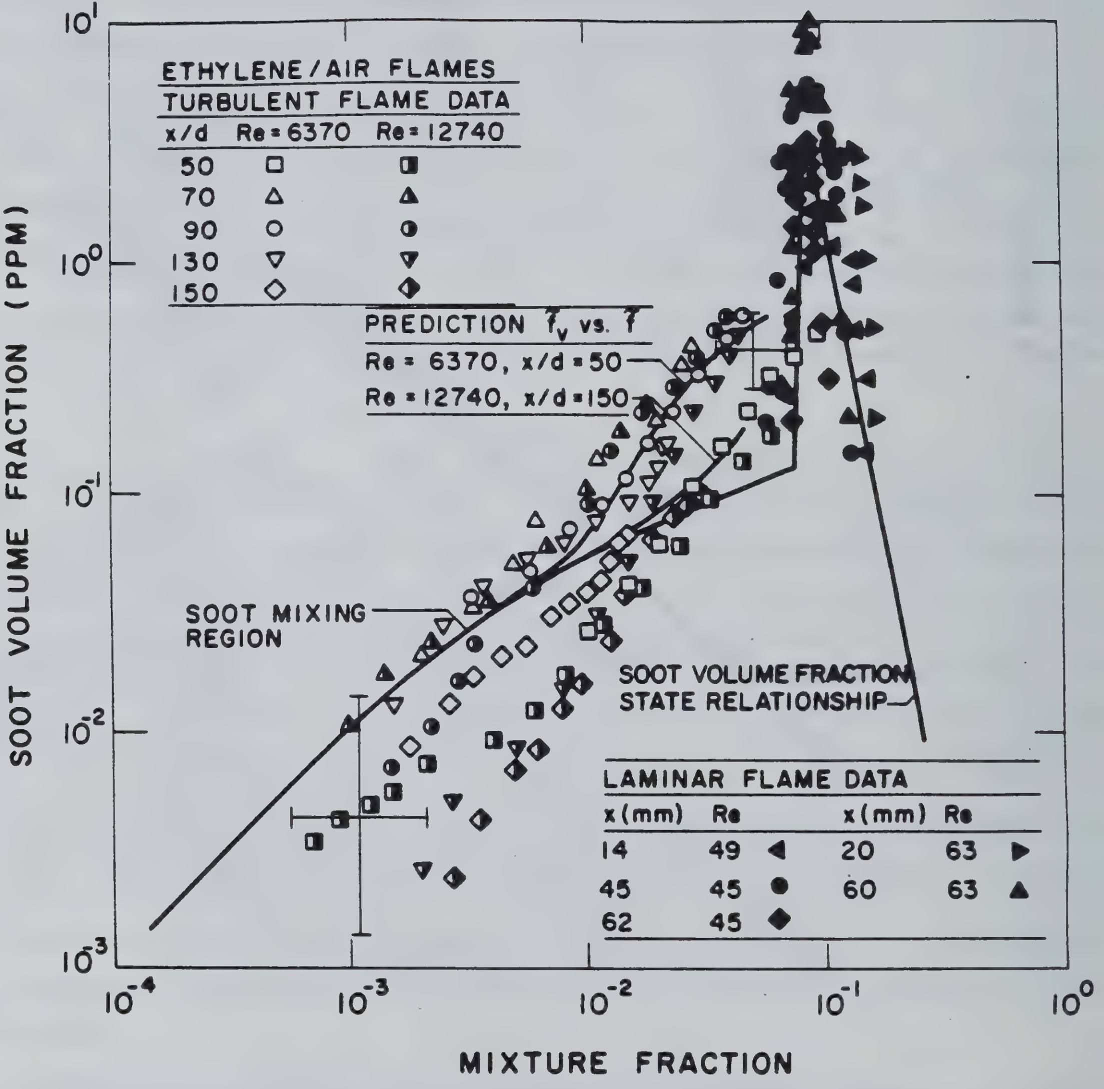

Figure 34. Soot volume fraction state relationships for ethylene/ air diffusion flames (the stoichiometric mixture fraction is 0.0634).

findings of Becker and Liang (1983), suggest significantly longer characteristic chemical times needed to reach the plateau region for soot generation efficiencies for ethylene than for acetylene. Since characteristic residence times vary for different paths through the flame, this would imply different soot volume fractions when soot oxidation is quenched; and different correlations of soot volume fractions as a function of mixture fraction, during subsequent passive mixing of soot in the overfire region. Thus, the results illustrated in Fig. 33 suggest potential for universal soot volume fraction state relationships for ethylene, but only at sufficiently large characteristic flame residence times. Additional measurements for a wider range of conditions, with better control of experimental uncertainties, will be needed for an adequate evaluation of the laminar flamelet concept for soot volume fractions, and the range of conditions where it applies.

3.4.3 Soot Generation Efficiencies

Soot generation efficiencies were computed for the overfire region of the test flames. The density of soot for these calculations was taken to be 1100 kg/m^3, which is the value recently found by Newman and Steciak (1987) for a variety of hydrocarbon fuels (including ethylene) in the overfire region of buoyant diffusion flames. Only results where analysis showed that effects of biasing due to turbulent fluctuations were relatively small were used ($f < 0.02$ for acetylene and $f < 0.01$ for ethylene, see Figs. 22 and 33). The results are summarized in Table 5. Since effects of finite-rate chemistry are suspected for the high Reynolds number ethylene flame, separate values are given using data from both flames, and only data from low Reynolds number flame. In addition to present measurements, other results summarized in Table 5 include: soot generation efficiencies inferred from the state relationships of Gore and Faeth (1987a,b), a value for ethylene reported by Newman and Steciak (1987), and values for both fuels obtained from the measurements of Becker and Liang (1982, 1983). Flame conditions for the Newman and Steciak (1987) result were not prescribed. The measurements from Becker and Liang (1983) are for the plateau region at longer characteristic residence times, where soot generation efficiencies were relatively independent of burner operating conditions. Becker and Liang (1983) found soot concentrations by sampling, while soot concentrations were found from extinction measurements for the other results summarized in Table 5.

Present measurements generally agree, within one standard deviation, with the other values listed in Table 5. As suggested by the results illustrated in Figs. 22 and 33, present soot generation efficiencies – considering all the flames – are somewhat lower than the values found by Gore and Faeth (1987a,b), while considering only the low Reynolds number ethylene flame yields values just slightly higher than those of Gore and Faeth (1987a). Soot generation efficiencies from the present study and Gore and Faeth (1987a) are 30-40 percent lower than the value reported by Newman and Steciak (1987) for ethylene. Aside from potential differences due to different flame conditions, interpretation of the extinction measurements could be responsible for this discrepancy. Newman and Steciak (1987) use Mie scattering theory and refractive indices for soot from Tien and Lee (1982), while present results are for the Rayleigh scattering approximation using refractive indices from Dalzell and Sarofim (1969). The effect of the Rayleigh scattering approximation is difficult to evaluate without information on soot particle size distributions, however, calculations of Santoro et al. (1983a,b) suggest reductions of present estimates of soot generation efficiencies by five to fifteen percent if Mie scattering theory was used. In contrast, use of the refractive indices of Tien and Lee (1982) would increase present estimates of soot volume fractions by 30-40 percent. In view of these considerations, the soot generation efficiency for ethylene reported by Newman and Steciak (1987) is reasonably consistent with the results from this laboratory. The sampling measurements of Becker and Liang (1983) are smaller than the optical measurements, particularly for ethylene; perhaps due to incomplete collection of soot, which is frequently a problem with sampling methods, or effects of additional uncertainties in soot densities.

Table 5. Soot Generation Efficiencies[a]

Source	Fuel	
	Ethylene	Acetylene
Present study[b,c]		
All flames	0.010 (0.006)	0.11 (0.07)
Low Reynolds number ethylene flame	0.012 (0.006)	------------
Gore and Faeth (1987a,b)[b]	0.012	0.21
Newman and Steciak (1987)[c]	0.017	------------
Becker and Liang (1982, 1983)[d]	0.004	0.10

[a] For diffusion flames in still air with reactants initially at normal temperature and pressure.

[b] Estimated from soot volume fraction measurements, using a soot density of 1100 kg/m^3, from Newman and Steciak (1987).

[c] Numbers in parentheses denote standard deviations.

[d] For characteristic residence times (as defined by Becker and Liang (1982, 1983)) greater than 180s for ethylene and 70s for acetylene.

The values of the overfire soot generation efficiency for acetylene are quite high, comparable to PVC and polystyrene (Newman and Steciak, 1987). If the overfire soot density is still appropriate for fuel-rich conditions, the earlier laminar flame measurements (see Fig. 34) suggest soot generation efficiencies on the order of 100 percent at the peak of the soot spike in the fuel-rich region. This value seems high and could be influenced by the effects of differential diffusion.[3] This near-saturation behavior, however, could explain why maximum soot volume fractions in laminar acetylene/air diffusion flames were relatively independent of height above the burner exit, in spite of shifts in the mixture fraction where the peak was observed.

Present findings, and the results of others summarized in Table 5, suggest that soot generation efficiencies of the luminous diffusion flames as a whole, and point-to-point within the overfire region, may be roughly constant when characteristic residence times are sufficiently large, i.e., in the plateau region observed by Becker and Liang (1983). This implies at least roughly universal soot volume fraction state relationships for the overfire region, which would be a very helpful property for radiation computations for luminous turbulent diffusion flames. Additional data, with reduced experimental uncertainties, are needed for a wider range of fuels, flame configurations and operating conditions, in order to adequately assess the potential of this simplification.

3.5 Summary

3.5.1 Conclusions

Scalar properties in the overfire (lean) region of turbulent ethylene and acetylene diffusion flames burning in air were considered both theoretically and experimentally. This is a report of progress for a continuing investigation. The major conclusions that can be drawn from the results thus far are as follows:

1. Mean concentrations of major gas species and mixture fractions were predicted reasonably well, similar to past experience with the present analysis for round turbulent diffusion flames (Gore and Faeth, 1987a,b; Gore et al., 1987a,b,c; Jeng and Faeth, 1987a,b; Jeng et al. 1982, 1984).

2. Consideration of both laminar and turbulent flames suggests nearly universal state relationships for major gas species, which closely approximate local thermodynamic equilibrium, in the overfire region of turbulent sooting acetylene and ethylene diffusion flames.

---

[3] Mass diffusivities of soot particles are small in comparison to gases, which would tend to trap excess fuel carbon in the soot layer.

3. Predictions of time-averaged soot volume fraction distributions in the turbulent flames, using soot volume fraction state relationships found earlier (Gore and Faeth, 1987a,b), were reasonably good in view of experimental uncertainties and the approximations of the analysis to find flame structure.

4. Direct evaluation of soot volume fraction state relationships for the overfire region was hampered by effects of turbulent fluctuations (near stoichiometric conditions) and large experimental uncertainties (for very lean conditions). Within these limitations, present findings support nearly constant soot generation efficiencies from point-to-point in the overfire region, at sufficiently large characteristic residence times, yielding soot volume fraction state relationships similar to earlier proposals (Gore and Faeth, 1987a,b). However, effects of finite-rate chemistry were noted at shorter residence times for ethylene, causing spatial variations of soot generation efficiencies (and, thus, the soot volume fraction state relationships) in the overfire region.

5. Present measurements of soot generation efficiencies, for flames having long characteristic residence times, were in fair agreement with earlier measurements based on optical methods, after considering effects of Mie scattering corrections and different correlations for soot refractive indices (Gore and Faeth, 1987a,b; Newman and Steciak, 1987); and with sampling measurements reported by Becker and Liang (1983).

3.5.2 Plans

Present findings suggest that soot volume fraction state relationships are potentially a useful concept which can help to circumvent the complexities of soot chemistry in turbulent flames in some instances, at least for the purpose of estimating soot properties for radiation predictions. The concept also provides a useful perspective from which to consider effects of finite-rate chemistry and transport on soot processes in turbulent flames. Further evaluation of the concept for a wider range of fuels and flame conditions appears to be warranted.

The main limitations of the present study involved excessively large experimental uncertainties at low mixture fractions, where effects of turbulent fluctuations are small; and excessive effects of turbulent fluctuations at near stoichiometric conditions due to presence of the soot spike, where intrinsic experimental uncertainties were more satisfactory. To avoid these difficulties, either improved experimental accuracy at low mixture fractions or capabilities for instantaneous mixture fraction and soot volume fraction measurements are needed.

Another limitation of the present study is that flame configurations were limited to buoyant jet diffusion flames. This configuration has the advantages of providing a flow where transition to turbulence in the flow field does not have to be considered, and the boundary layer approximations apply, simplifying computations. Nevertheless, geometries more like those encountered in fires, and larger-scale flames, should be considered in order to test the laminar flamelet concept for soot volume fractions. Finally, a variety of fuels should be considered, ranging from moderately to heavily sooting fuels, so that effects of finite-rate chemistry on soot concentrations in buoyant turbulent diffusion flames can be assessed. Work along these lines is currently in progress in this laboratory.

REFERENCES

Aeschliman, D. P., Cummings, J. C. and Hill, R. A. (1979) Raman spectroscopic study of a laminar hydrogen diffusion flame in air. J. Quant. Spectrosc. Radiat. Trans. 21, 293-307.

Becker, H. A. and Liang, D. (1982) Total emission of soot and thermal radiation by free turbulent diffusion flames. Comb. Flame 44, 305-318.

Becker, H. A. and Liang, D. (1983) Soot emission, thermal radiation, and laminar instability of acetylene diffusion flames. Comb. Flame 52, 247-256.

Becker, H. A., Hottel, H. C. and Williams, G. C. (1967) The nozzle-fluid concentration field of the round, turbulent, free jet. J. Fluid Mech. 30, 285-303.

Bilger, R. W. (1976) Reaction rates in diffusion flames. Comb. Flame 30, 277-284.

Bilger, R. W. (1977) Turbulent jet diffusion flames. Prog. Energy Combust. Sci. 1, 87-109.

Box, G.E.P. and Jenkins, G. M. (1976) Time Series Analysis, Holden-Day, San Francisco.

Cox, G. (1977) On radiant heat transfer from turbulent flames. Comb. Sci. Tech. 17, 75-78.

Dalzell, W. H. and Sarofim, A. F. (1969) Optical constants of soot and their application to heat-flux calculations. J. Heat Transfer 91, pp. 100-104.

de Ris, J. (1978) Fire radiation – a review. Seventeenth Symposium (International) on Combustion, The Combustion Institute, Pittsburgh, 1003-1016.

Drake, M. C., Lapp, M., Penney, C. M. and Warshaw, S. (1980) Measurements of temperature and concentration fluctuations in turbulent diffusion flames using pulsed Raman spectroscopy. Eighteenth Symposium (International) on Combustion, The Combustion Institute, Pittsburgh, 1521-1531.

Drake, M. C., Pitz, R. W. and Lapp, M. (1984) Laser measurements of nonpremixed hydrogen-air flames for assessment of turbulent combustion models. AIAA Paper No. 84-0544.

Faeth, G. M. and Samuelsen, G. S. (1986) Fast-reaction nonpremixed combustion. Prog. Energy Combust. Sci. 12, 305-372.

Gordon, S. and McBride, B. J. (1971) Computer program for calculation of complex chemical equilibrium compositions, rocket performance, incident and reflected shocks, and Chapman-Jouguet detonations. NASA SP-273.

Gore, J. P. (1986) A theoretical and experimental study of turbulent flame radiation. Ph.D. Thesis, The Pennsylvania State University, University Park, PA.

Gore, J. P. and Faeth, G. M. (1987a) Structure and spectral radiation properties of turbulent ethylene/air diffusion flames. Twenty-First Symposium (International) on Combustion, The Combustion Institute, Pittsburgh, in press.

Gore, J. P. and Faeth, G. M. (1987b) Structure and radiation properties of luminous turbulent acetylene/air diffusion flames. J. Heat Trans., in press.

Gore, J. P., Faeth, G. M., Evans, D. and Pfenning, D. (1987a) Structure and radiation properties of large-scale natural gas/air diffusion flames. Fire and Materials, 10, 161-169.

Gore, J. P., Jeng, S.-M. and Faeth, G. M. (1987b) Spectral and total radiation properties of turbulent carbon monoxide/air diffusion flames. AIAA J. 25, 339-345.

Gore, J. P., Jeng, S.-M. and Faeth, G. M. (1987c) Spectral and total radiation properties of turbulent hydrogen/air diffusion flames. J. Heat Trans. 109, 165-171.

Gore, J. P., Kounalakis, M. E. and Faeth, G. M. (1987d) Temporal properties of radiation fluctuations from nonluminous turbulent diffusion flames. Proceedings of the Twentieth Fall Technical Meeting, Eastern Section of the Combustion Institute, Pittsburgh, 71.1-71.4.

Grosshandler, W. L. (1980) "Radiative heat transfer in nonhomogeneous gases: a simplifed approach," Int. J. Heat Mass Transfer 23, pp. 1447-1457.

Jeng, S.-M. and Faeth, G. M. (1984a) Species concentrations and turbulence properties in buoyant methane diffusion flames. J. Heat Trans. 106, 721-727.

Jeng, S.-M. and Faeth, G. M. (1984b) Predictions of mean scalar properties in turbulent propane diffusion flames. J. Heat Trans. 106, 891-893.

Jeng, S.-M. and Faeth, G. M. (1984c) Radiative heat fluxes near turbulent buoyant methane diffusion flames. J. Heat Trans. 106, 886-888.

Jeng, S.-M., Chen, L.-D. and Faeth, G. M. (1982) The structure of buoyant methane and propane diffusion flames. Nineteenth Symposium (International) on Combustion, The Combustion Institute, Pittsburgh, 949-958.

Jeng, S.-M., Lai, M.-C. and Faeth, G. M. (1984) Nonluminous radiation in turbulent buoyant axisymmetric flames. Comb. Sci. Tech. 40, 41-52.

Kabashnikov, V. P. and Kmit, G. I. (1979) Influence of turbulent fluctuations on thermal radiation. J. Appl. Spect. 31, 963-967.

Kent, J. H. (1987) Turbulent diffusion flames sooting-relationship to smoke-point tests. Comb. Flame 67, 223-233.

Kent, J. H. and Bastin, S. J. (1984) Parametric effects on sooting in turbulent acetylene diffusion flames. Comb. Flame 56, 29-42.

Lai, M.-C. and Faeth, G. M. (1987) Turbulence structure of vertical adiabatic wall plumes. J. Heat Trans. 109, 663-670.

Liew, S. K., Bray, K.N.C. and Moss, J. B. (1981) A flamelet model of turbulent non-premixed combustion. Comb. Sci. Tech. 27, 69-73.

Ludwig, C. B., Malkmus, W., Reardon, J. E. and Thomson, J. A. (1973) Handbook of Infrared Radiation from Combustion Gases, NASA SP-3080.

Miller, J. A. and Kee, R. J. (1977) Chemical nonequilibrium effects in hydrogen-air laminar jet diffusion flames. J. Phys. Chem. 81, 2534-2542.

Newman, J. S. and Steciak, J. (1987) Characterization of particulates from diffusion flames. Comb. Flame 67, 55-64.

Pagni, P. J. and Bard, S. (1979) Particulate volume fractions in diffusion flames. Seventeenth Symposium (International) on Combustion. The Combustion Institute, Pittsburgh, 1017-1026.

Pagni, P. J. and Okoh, C. I. (1984) Soot generation within radiating diffusion flames. Twentieth Symposium (International) on Combustion, The Combustion Institute, Pittsburgh, PA, 1985, pp. 1045-1054.

Portscht, R. (1978) Studies on characteristic fluctuations of flame radiation emitted by fires. Comb. Sci. Tech. 10, 73-84.

Santoro, R. J., Dobbins, R. A. and Semerjian, H. G. (1983a) Interpretation of optical measurements of soot in flames. AIAA Paper No. 83-1516.

Santoro, R. J., Semerjian, H. B. and Dobbins, R. A. (1983b) Soot particle measurements in diffusion flames. Comb. Flame 51, 203-218.

Shaughnessy, E. J. and Morton, J. B. (1977) Laser light-scattering measurements of particle concentration in a turbulent jet. J. Fluid Mech. 80, 129-148.

Spalding, D. B. (1977) GENMIX: A General Computer Program for Two-Dimensional Parabolic Phenomena, Pergamon Press, Oxford.

Stårner, S. H. and Bilger, R. W. (1980) Measurements of scalar-velocity correlations in a turbulent diffusion flame. Eighteenth Symposium (International) on Combustion, The Combustion Institute, Pittsburgh, 921-930.

Tien, C. L. and Lee, S. C. (1982) Flame radiation. Prog. Energy Combust. Sci. 8, 41-59.

FORM NBS-114A (REV.11-84)

U.S. DEPT. OF COMM. **BIBLIOGRAPHIC DATA SHEET** (See instructions)	1. PUBLICATION OR REPORT NO. NIST/GCR-88/553	2. Performing Organ. Report No.	3. Publication Date October 1988

4. TITLE AND SUBTITLE

Radiation from Turbulent Nonluminous and Luminous Diffusion Flames

5. AUTHOR(S)

Y.R. Sivathanu, M.E. Kounalakis, J.P. Gore and G.M. Faeth

6. PERFORMING ORGANIZATION *(If joint or other than NBS, see instructions)*

University of Michigan
Dept. of Aerospace Engineering
Ann Arbor, MI

7. Contract/Grant No.

8. Type of Report & Period Covered

9. SPONSORING ORGANIZATION NAME AND COMPLETE ADDRESS *(Street, City, State, ZIP)*

National Institute of Standards
and Technology
U.S. Department of Commerce
Gaithersburg, MD 20899

10. SUPPLEMENTARY NOTES

☐ Document describes a computer program; SF-185, FIPS Software Summary, is attached.

11. ABSTRACT *(A 200-word or less factual summary of most significant information. If document includes a significant bibliography or literature survey, mention it here)*

A theoretical and experimental study of the structure and radiation properties of turbulent buoyant diffusion flames is described. The results have application to modeling the fires within structures, materials test methods, fire detection, and effects of materials on fire properties. Issues concerning turbulent-radiation interactions in nonluminous flames and application of laminar flamelet concept to soot volume fractions for heavily sooting flames were addressed. Measurements of transient radiation intensities provided direct experimental evidence of turbulence-radiation interactions. The temporal power spectra of radiation intensity show energy containing and inertial regions similar to other turbulence properties. A stochastic model based on time-series analysis and the laminar flamelet concept was developed and provided encouraging predictions of fluctuating radiation properties. Measurements of soot volume fractions and mixture fractions in turbulent flames particularly in the overfire regions were completed. Direct evaluation of the state relationship concept for soot volume fractions is hampered by turbulent fluctuations and experimental uncertainties. However, trends show that for long residence times the soot generation efficiencies are fairly constant and that the universal state relationships are possible. The values of soot generation efficiencies were also in agreement with past results from this laboratory and from literature.

12. KEY WORDS *(Six to twelve entries; alphabetical order; capitalize only proper names; and separate key words by semicolons)*

diffusion flames; radiation; soot; turbulent flames

13. AVAILABILITY

☒ Unlimited
☐ For Official Distribution. Do Not Release to NTIS
☐ Order From Superintendent of Documents, U.S. Government Printing Office, Washington, DC 20402.
☒ Order From National Technical Information Service (NTIS), Springfield, VA 22161

14. NO. OF PRINTED PAGES

91

15. Price

$13.95